crystals

MDPI

Review

Advanced Preparation Methods for Ceramic Membrane Materials in Electrochemical Applications

Keqiang Fan [1,2], Mengyang Yu [1,2], Jincheng Lei [3,*] and Shenglong Mu [1,2,*]

[1] Liaoning Provincial Key Laboratory for Preparation and Application of Special Functional Materials, Shenyang University of Chemical Technology, Shenyang 110142, China; fanfankeqiang@gmail.com (K.F.); 15904059519@163.com (M.Y.)
[2] Shenyang Key Laboratory for New Functional Coating Materials, Shenyang University of Chemical Technology, Shenyang 110142, China
[3] Shien-Ming Wu School of Intelligent Engineering, South China University of Technology, Guangzhou 511442, China
* Correspondence: leijincheng@scut.edu.cn (J.L.); smu@syuct.edu.cn (S.M.)

Abstract: The outstanding thermal, chemical, and mechanical properties of ceramic membranes have attracted increasing attention, offering advantages over polymer and metal counterparts. Exploring the specialized applications of ceramic membranes through various preparation methods poses a daunting challenge for contemporary researchers. Traditional preparation methods are essentially unable to meet the requirements of complex membrane structures. For instance, in ceramic fuel cell applications, cells composed of ceramic membrane materials exhibit high resistance and low conductivity, which seriously hinders the progress of new high-performance ceramic fuel cells. Therefore, it is necessary to improve preparation methods to improve the electrochemical performance of devices composed of ceramic membrane materials. In recent years, breakthroughs in various new processing technologies have propelled the performance of ceramic membrane devices. This paper will focus on the following aspects. Firstly, traditional preparation methods and advanced preparation methods of ceramic membrane materials will be discussed. Secondly, high-performance ceramic membrane materials prepared by different advanced preparation methods are introduced, and the electrochemical properties of the devices composed of ceramic membrane materials are elaborated in combination with different testing and characterization methods. Finally, the prospects and future direction of the preparation of ceramic membrane materials by advanced preparation methods are summarized.

Keywords: ceramic membrane; advanced fabrication methods; electrochemical properties; ceramic fuel cell; conductivity

Citation: Fan, K.; Yu, M.; Lei, J.; Mu, S. Advanced Preparation Methods for Ceramic Membrane Materials in Electrochemical Applications. *Crystals* **2024**, *14*, 623. https://doi.org/10.3390/cryst14070623

Academic Editor: Vladislav V. Kharton

Received: 24 April 2024
Revised: 27 May 2024
Accepted: 4 July 2024
Published: 6 July 2024

1. Introduction

In contemporary society, ceramic membrane materials have extensive applications in the field of electrochemistry, showcasing significant advantages and potential. Compared to polymer membranes, ceramic membranes generally have higher mechanical strength and tensile resistance, making them less susceptible to physical damage or fracture and suitable for applications requiring high stability and durability. These materials possess excellent chemical and thermal stability, allowing them to operate reliably in high-temperature, high-pressure, and corrosive environments, making them the optimal choice for electrochemical reactors and fuel cells [1,2]. Their high ionic conductivity and selective permeability are crucial for enhancing the efficiency of electrochemical devices. For instance, in water electrolysis for hydrogen production, ceramic membranes can efficiently separate hydrogen and oxygen, increasing the efficiency and purity of hydrogen production [3–5]. Moreover, ceramic membranes exhibit exceptional catalytic performance in electrocatalytic processes,

improving the rate and selectivity of these reactions [6–8]. Consequently, ceramic membrane materials hold broad application value in the field of electrochemistry.

Embarking from the application of ceramic membrane materials, it becomes imperative to comprehend the requisite structural features and performance demands. For instance, in the realm of electrocatalysis, ceramic membrane materials are characterized by their high specific surface area and porous structure, coupled with the requisite electrochemical property of excellent conductivity. These attributes collectively furnish an abundance of active sites, thereby facilitating the transport of reactants and products and enhancing catalytic efficiency. Moreover, the mechanical and chemical stability of ceramic membranes is of paramount importance in electrocatalytic environments, ensuring their durability and sustained performance [7,9,10]. In addition, in the field of ceramic fuel cell applications, ceramic electrolyte membranes need to be dense to prevent gas mixing [11]. Thereinto, ceramic membranes typically exhibit excellent high-temperature stability, capable of operating at elevated temperatures without failure. This gives ceramic membranes an advantage in high-temperature electrochemical applications such as solid oxide fuel cells (SOFCs) [12]. Ceramic membrane materials need to possess high ion transport performance, chemical stability, and enclosed gas channels for efficient conversion and stability during electrolysis. To meet these requirements, membranes are typically fabricated as thin layers on porous substrates [13]. The primary function of these porous substrates is to provide structural support and increase the surface area of the electrolyte layer to facilitate ion transport. Common porous substrates used in high-temperature electrolyte applications such as SOFCs include zirconia, magnesia, etc. These materials exhibit excellent high-temperature stability and mechanical strength, making them suitable as support structures for ceramic electrolyte membranes [14–16]. In addition to performance, factors such as long-term stability under corrosive conditions, mechanical loads, and membrane-housing technology are crucial for future applications [17].

However, there are some challenges and barriers related to the preparation technology necessary to achieve these required structural features and performance requirements. The traditional technical routes for the preparation of ceramic membranes are mainly as follows: pressing [18,19], extrusion [20], spinning [21], dip coating [22], tape casting [23], and freeze casting [24]. The drawbacks of traditional methods for fabricating ceramic membranes include the following: high production costs, high energy consumption, long production cycles, and complex preparation processes. Therefore, it is difficult for traditional preparation techniques to meet the requirements of complex ceramic membrane structures, which limits the development of ceramic membranes. In view of the inadequacy of traditional ceramic membrane material preparation methods, researchers have developed many advanced preparation processes. For example, additive manufacturing (AM), commonly referred to as 3D printing, is a process that involves building parts layer by layer using 3D design data [25]. Under the impetus of digital technology, 3D printing has been widely used [26,27]. Three-dimensional printing is a bottom-up preparation process [28,29]. Three-dimensional printing has shown obvious characteristics in the production and structural and functional design of ceramic membranes [30,31]. Three-dimensional printing has emerged as an innovative means for the rapid fabrication of high-performance thin films, garnering widespread attention in recent years. The structure of ceramic membranes can be improved by using 3D printing. Furthermore, chemical vapor deposition (CVD) and physical vapor deposition (PVD) are commonly used techniques for manufacturing ceramic thin films. CVD enables high purity, uniformity, and complex structure, suitable for large-area film fabrication. PVD offers excellent film density and control over the ceramic lattice, making it suitable for small-sized and complex-shaped films. Both methods allow the preparation of stable ceramic films at high temperatures, contributing to enhanced performance and reliability [32,33]. Subsequently, the electrochemical properties of the ceramic membranes fabricated by advanced preparation technology were tested. This paper focuses on the latest discussions and advancements in the preparation of ceramic membrane materials,

encompassing various manufacturing methods, membrane structures, and applications. Summaries of their respective characterization results are provided.

2. Manufacturing Method of Ceramic Membrane Materials

Traditional methods for manufacturing ceramic membrane materials for electrochemical applications include the pressing method, extrusion method, phase-inversion method, slip casting method, tape casting method, and others. These methods involve mixing ceramic powders with additives, forming thin film structures through specific processing steps, and finally drying and sintering to obtain the desired ceramic membrane products. Tight control of parameters is required during the preparation process to achieve high membrane quality. The drawbacks of traditional methods for manufacturing ceramic membranes include complexities in processing, long production cycles, high costs, difficulty in precision control, shape limitations, susceptibility to cracking and deformation, among others [34].

To overcome the limitations of traditional methods and enhance the performance of ceramic films, various approaches can be adopted. Exploring and developing novel ceramic materials such as composite materials and nanomaterials can improve film performance. Innovative processing methods can also be designed to achieve more precise structural control, higher product consistency, and shorter production cycles, thereby enhancing the quality and performance of ceramic films. Optimizing manufacturing processes can improve production efficiency and product quality. Through structural design and engineering control, precise design and engineering control can be utilized to optimize film performance [35].

Among these methods, innovative processing methods offer many advantages in improving the quality of ceramic membranes. They typically enable precise control over the structure of ceramic membrane materials, allowing the adjustment of key structural parameters such as density through precise process parameters and processing techniques, thus facilitating fine-tuning of membrane performance. Furthermore, precise control and treatment can improve membrane surface properties, structural characteristics, and chemical stability, thereby enhancing performance in specific application scenarios [36]. The following section will primarily introduce advanced manufacturing methods for ceramic membrane materials.

2.1. Conventional Processing Technology for Ceramic Membrane Materials

2.1.1. Pressing Method

The pressing method is a common technique for making ceramic films. It involves using suitable ceramic powders that are processed and shaped in molds under pressure. This process causes the ceramic particles to deform and bond together, forming a dense precursor. The precursor is then sintered at high temperatures to further bond and crystallize the particles, resulting in a dense ceramic structure. Despite its effectiveness, drawbacks include multiple steps, higher costs, limited shape complexity, and challenges with precision and thickness control [13,19]. Chakraborty et al. [37], by employing raw materials such as feldspar, sawdust, and kaolin, along with various chemicals including sodium silicate, fabricated low-cost, carbonate-free membranes using the pressing method. Analysis revealed that these membranes exhibited flawless characteristics, showcasing a uniform surface structure with evenly distributed pores of similar dimensions. Ivanets et al. [38], using quartz sand with a particle size ranging from 200 to 630 μm, along with raw materials such as sodium aluminum silicate, flour, starch, cellulose, and ethoxyethanol, fabricated membranes via the radial compression molding method. Through this pressing approach, the porosity can achieve 30–34%.

2.1.2. Extrusion Method

Extrusion is a conventional technique for the production of ceramic membranes. Its principle involves selecting appropriate ceramic powders as raw materials, which are mixed

with additives and solvents to form a slurry. The slurry is then injected into molds or an extrusion machine of specific shapes, where it is subjected to pressure and extruded to form a continuous thin film structure along the predetermined direction. Additionally, desired film shapes and dimensions can be achieved through mold design. The extruded ceramic film is dried to remove solvents and moisture, with precise control during drying being crucial to prevent film rupture or deformation. Finally, the dried ceramic film undergoes sintering to bond particles into a dense ceramic structure. The sintering process must occur under appropriate temperature and time conditions to ensure the final performance and stability of the film. Through these steps, extrusion can be utilized to prepare ceramic films with specific shapes and dimensions [39,40]. This method offers a simple process and relatively low costs, making it suitable for large-scale membrane production. However, it is essential to carefully control the parameters during the extrusion process to ensure membrane quality [20]. Figure 1 illustrates the process flow of the extrusion method.

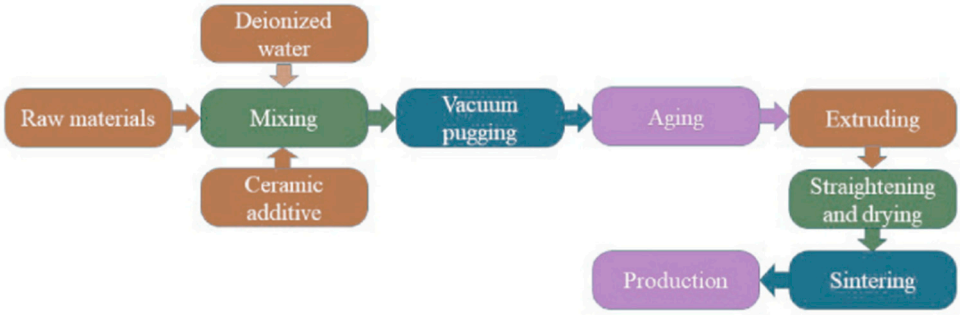

Figure 1. Flow chart of extrusion method. Reprinted with permission from Ref. [20]. Copyright 2021 Elsevier.

Suresh et al.'s [41] ceramic membranes prepared using the extrusion method exhibit excellent characteristics, with pore sizes of 1.4 lm. Similarly prepared membranes also demonstrate approximately 35% porosity and excellent mechanical stability of 1.68 MPa. Meghnani et al.'s [42] preparation of ceramic membranes using various inexpensive precursors is explored. The authors employed different sintering temperatures during the synthesis process, opting for 900 °C as the optimal temperature. Utilizing the compaction method, the porosity ranged from 41% to 36%, while the pore size varied from 0.52 to 1.78 lm [42].

2.1.3. Phase-Inversion Method

The phase-inversion method is as a technique for fabricating ceramic membranes, realized through the sol–gel process. Figure 2 depicts a schematic diagram of the phase transformation casting technique: The degassed suspension is first poured into the casting equipment and the device is placed on the surface of the water to maintain contact with the water (Figure 2A). After that, the piston is pushed into the water at a constant speed, and the suspension undergoes a phase conversion process and is not fully solidified in the water (Figure 2B). The partially cured tubular membrane is then immersed in water for 48 h for fur-ther curing (Figure 2C). Finally, a tubular membrane is obtained after removal on the piston (Figure 2D). Prepare a sol–gel solution containing metal ions or precursors composed of organic or inorganic materials. Then, finely coat the solution onto a substrate to form a thin layer. Subsequently, dry the coating to facilitate solvent evaporation, resulting in the formation of a gel layer. The critical step involves heat treatment, catalyzing the conversion of organic components in the sol–gel into an inorganic phase, thereby forming a ceramic film. Post-treatment may include surface modification. Ceramic films prepared via phase transformation methods exhibit a dense structure and excellent chemical stability, suitable for applications in thin film separation, sensors, and catalysis. Advantages include a simple preparation process, lower cost, and the ability to control film thickness and porosity [43].

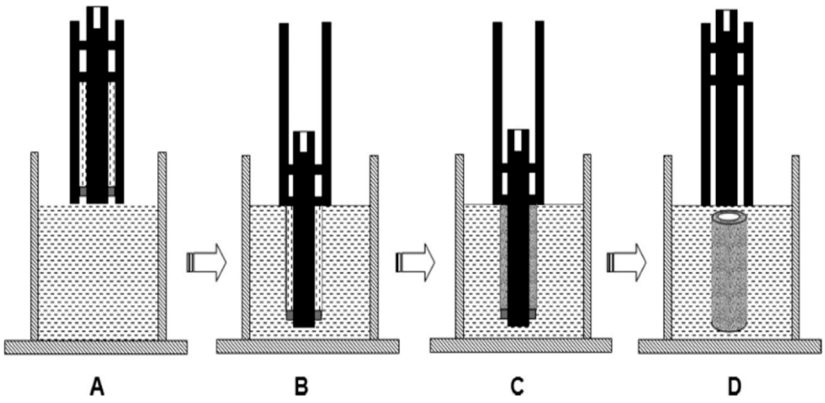

Figure 2. Schematic representation of the phase-inversion casting technique. Reprinted with permission from Ref. [44]. Copyright 2015 Elsevier.

Zhu et al. [44] proposed introduced a groundbreaking casting method to fabricate tubular ceramic membranes using self-designed molding tools and preparation routes. The manufactured ceramic membranes were characterized through pore size distribution, image analysis, porosity, mechanical strength, and gas flux measurements. The practical feasibility of a transformative casting process for the manufacture of tubular ceramic membranes was demonstrated.

2.1.4. Slip Casting Method

The slip casting method is a common technique for preparing ceramic film materials. The process involves selecting suitable ceramic powders and mixing them with additives, solvents, etc., to form a slurry. The slurry is then poured into molds or an extrusion machine of specific shapes. Within the molds, the slurry is subjected to pressure and extruded through mold openings to form a continuous thin film structure along a predetermined direction. Film formation and thickness are controlled by adjusting parameters such as extrusion speed, pressure, and temperature. The extruded ceramic film is dried to remove solvents and moisture. Finally, the dried ceramic film undergoes sintering to bond particles into a dense ceramic structure. The sintering process must occur under appropriate temperature and time conditions to ensure the final performance and stability of the film. Through these steps, the slurry casting method can be used to prepare ceramic films with specific shapes and dimensions [45,46].

2.1.5. Tape Casting Method

The tape casting method is a widely used manufacturing technique for ceramic film materials. Its principle involves mixing ceramic powders with additives and suspending them in an appropriate solvent to form a slurry. This slurry is uniformly coated onto a supported substrate, with control over coating speed and thickness to ensure the formation of a uniform ceramic film layer on the substrate surface. Utilizing methods such as heat treatment or chemical reactions, a dense ceramic film is generated on the substrate surface of the film material, ultimately producing the desired ceramic film material [47]. Ceramic membranes prepared via tape casting exhibit characteristics of structural density, high molding precision, and smooth surface finish, finding extensive applications in fields such as filtration membranes and separation membranes [48].

Nandini et al. [49] utilized tape casting technology to fabricate alumina membrane filters with diameters ranging from 25 to 30 mm and thicknesses between 0.3 and 0.8 mm, tailored for microfiltration applications. In the Table 1, Compares different traditional manufacturing methods for the fabrication of ceramic membrane materials.

Table 1. Comparison of different traditional methods.

Preparation Method	Applications	Structural	Merit	Drawbacks	References
Pressing	Membrane separation, Biomedicine	Evenly spaced holes	Simple, Low cost	Limited pore size distribution, Limited molding	
Extrusion	Electronics, Energy	Dense structural geometry	High control aperture accuracy, High production efficiency	Complex equipment and process, Molding limitations	
Phase-inversion	Hollow fiber membrane fabrication	Single multilayer formation	Higher interconnectivity	Limitation of membrane thickness	[50,51]
Slip casting	To produce scaffold	Interconnected porous layer	High pore size and porosity	Limitation of membrane thickness	[52]
Tape casting	Energy field, Environmental protection field	Homogeneous and continuous sheet-like structure	High molding flexibility, Low cost	Difficult pore size control, Limited film thickness	
Electrospinning	Support layer production	Non-woven nanofibrous mat	High surface area to volume ratio	Insufficient mechanical strength	[53,54]
Aerosol-assisted chemical vapor deposition	Biomedical, Catalysts	Homogeneous dense film, Porous film	Simple, Low cost	Slower, complex gas-phase reactions to prepare	
Physical vapor deposition	Hard coating, Optical coating	Dense or non-porous structures	High compactness and purity	Limited to a uniform surface	

2.2. Advanced Manufacturing Methods

Three-Dimensional Printing

Presently, photopolymerization-based printing technologies, categorized into stereolithography (SLA) and Digital Light Processing (DLP) based on the mode of formation, represent a form of rapid prototyping method, well-suited for fabricating intricate, small-scale, and hollow structures. The operational principles are depicted in Figure 3.

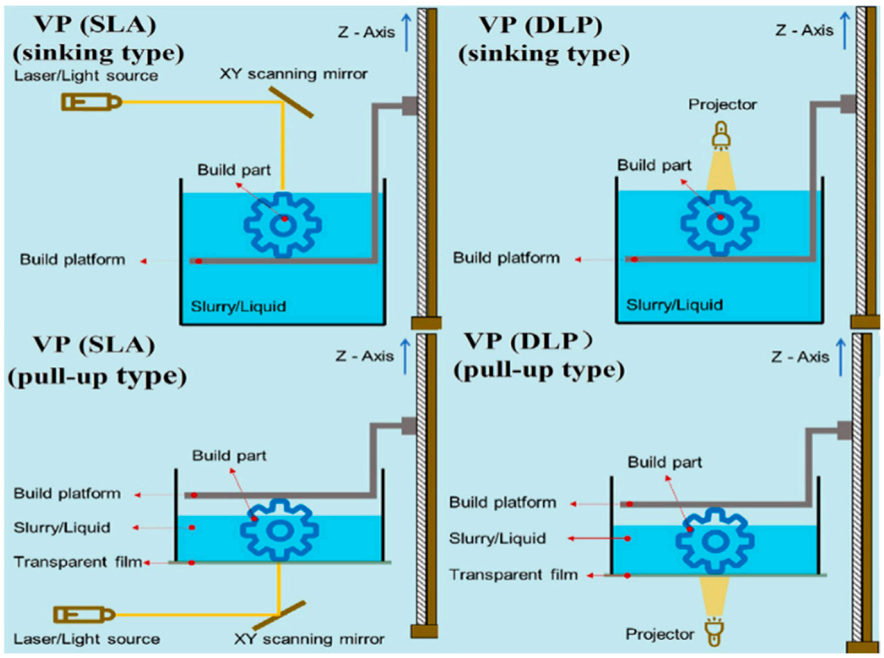

Figure 3. Schematic diagram of ceramics printed using SLA and DLP technology. Reprinted from Ref. [55].

The SLA technique [56] is an additive manufacturing technique for creating intricate three-dimensional microstructures. Its core principle lies in the photopolymerization of photosensitive materials, where UV light or laser selectively cures liquid photopolymer

resin layer by layer. The process unfolds as follows: Within a container of photosensitive resin, a computer-controlled UV light or laser scans the resin surface, selectively curing it according to a predetermined, two-dimensional, cross-sectional pattern. Subsequently, the platform descends by a minute layer thickness, and the scanning and curing process repeats. This cycle continues until the entire three-dimensional structure is complete. This stereolithography technique enables high-precision, high-resolution manufacturing of ceramic film materials, making it suitable for producing various complex structural devices [57].

Masciandaro et al. [58] utilized SLA technology to 3D print yttria-stabilized zirconia (YSZ) electrolyte membranes with honeycomb structures, significantly enhancing the physical properties of the membranes. Arianna et al. [59], using SLA technology, prepared a ripple-shaped YSZ electrolyte membrane (Figure 4a). The surface area of the membrane significantly increased compared to the planar shape, and the dimensions did not change.

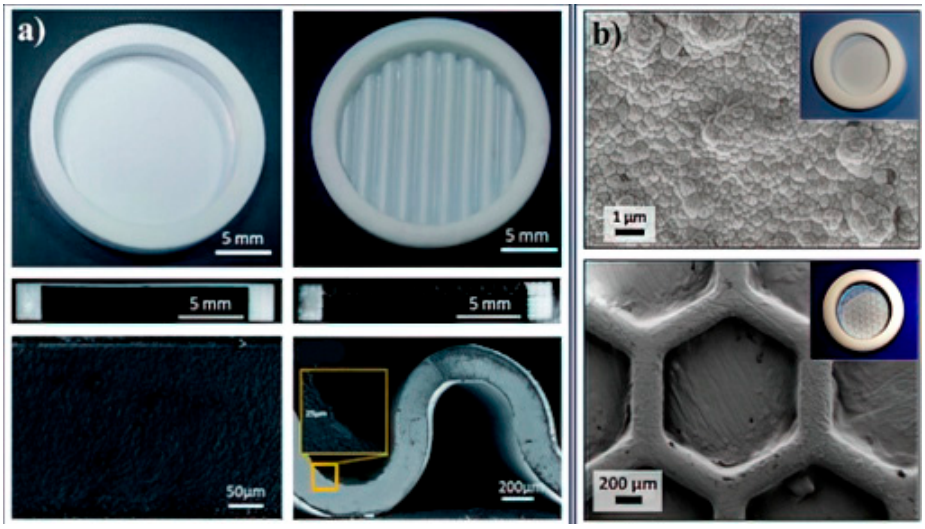

Figure 4. (**a**) SEM image of a corrugated YSZ ceramic membrane. (**b**) Honeycomb-shaped SEM image of YSZ ceramic membrane. Reprinted from Ref. [55].

DLP technology offers faster printing speeds, higher resolution, larger build volumes, simplified mechanical structures, and lower costs. DLP is capable of simultaneously processing entire layers, providing higher resolution and larger build volumes, with simpler mechanical structures and lower costs [60–62]. Depending on the direction of light source incidence, DLP technology can also be categorized into bottom-up and top-down approaches. The printing accuracy of DLP depends mainly on the size of the projected pixel block, typically controllable to around 50 μm, comparable to the printing precision of SLA. DLP rapid prototyping technology finds extensive application in the fabrication of structural ceramics such as SiO_2, Al_2O_3, and ZrO_2 [63–69].

Xing et al. [70,71], using DLP technology, 3D printed a ripple-shaped yttrium-oxide-stabilized zirconia electrolyte membrane. The contact area between the film and the electrode is significantly improved compared to a planar film of the same thickness, and the electrochemical performance of the device is enhanced (Figure 4b). Chen et al. [62], utilizing DLP technology, fabricated ZrO_2, all-ceramic dental prostheses using Y_2O_3-doped nano-ZrO_2 powder, achieving an approximate relative density of 98%.

The working principle of continuous liquid interface production (CLIP) is shown in Figure 5. Continuous CLIP technology utilizes a process called photopolymerization to produce ceramic membrane materials. In this technique, a UV light is projected through an oxygen-permeable window into a reservoir containing a photosensitive liquid resin. The oxygen inhibits the polymerization process near the window, creating a thin layer of uncured resin between the window and the liquid resin. As the UV light cures the resin layer, the build platform slowly rises, pulling the cured resin upward while maintaining a

continuous liquid interface. This process allows for the continuous fabrication of ceramic membranes with precise control over the shape and structure. CLIP technology enables the rapid production of ceramic membrane materials with high resolution and smooth surface finish, suitable for various applications in industries such as aerospace, medical, and energy.

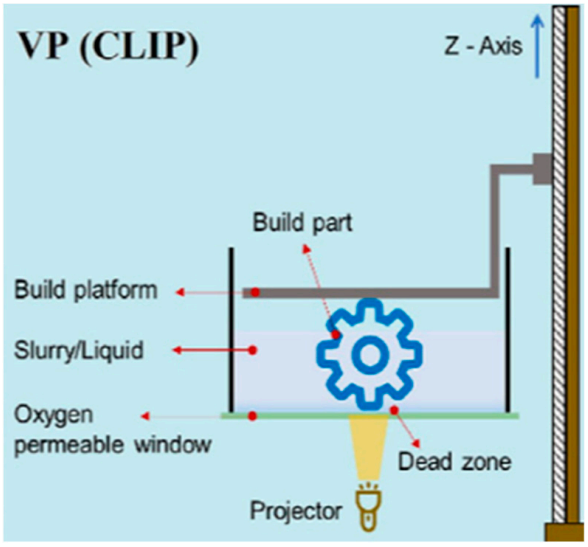

Figure 5. Schematic representation of ceramic 3D printing technology utilizing the CLIP technique. Reprinted from Ref. [55].

The Directed Energy Deposition (DED) technique is a method for fabricating ceramic membrane materials [72]. Figure 6 is a schematic diagram of the directional energy deposition device. In this process, high-energy sources such as lasers or electron beams are directed onto ceramic powder, causing it to melt instantly and deposit onto the substrate surface. With the movement of the energy source and the deposition of ceramic powder, the desired ceramic membrane material gradually forms. The entire process is computer-controlled, ensuring precise printing based on the designed three-dimensional model. DED technology offers advantages such as high precision, fast fabrication speed, and suitability for complex structures. It can produce ceramic membrane materials with excellent performance in a relatively short time, making it widely applicable in aerospace, medical, energy, and other fields.

Laser Engineered Net Shaping (LENS) printing technology offers the following advantages: minimal material waste, producing cost savings; capability to print complex structures, enhancing design flexibility; suitability for various materials, including high-performance alloys; repairs and refurbishes parts, extending their lifespan; high production efficiency, reducing manufacturing cycles; and being ideal for demanding sectors like aerospace and healthcare [73].

Mu et al. [75], through investigation into a novel, self-built integrated workstation featuring picosecond laser-CO_2, laser-3D printing, developed a new processing route from low-cost oxide and carbonate materials. This route enables additive manufacturing, laser-assisted rapid sintering, laser-assisted microprocessing, and structural morphology control, as depicted in Figure 7. This approach builds upon the rapidly evolving fields of 3D printing/additive manufacturing (AM) and laser processing (LP). Specifically, it involves layer-by-layer construction of pre-designed 3D models, with final sintering and structural shaping achieved through the assistance of lasers with different functionalities. The distinctive feature of laser 3D printing (L3DP) lies in the use of commercial raw materials, minimal binding agents, and rapid in situ drying facilitated by CO_2 lasers. L3DP technology has achieved rapid direct digital manufacturing based on ceramics [76–78].

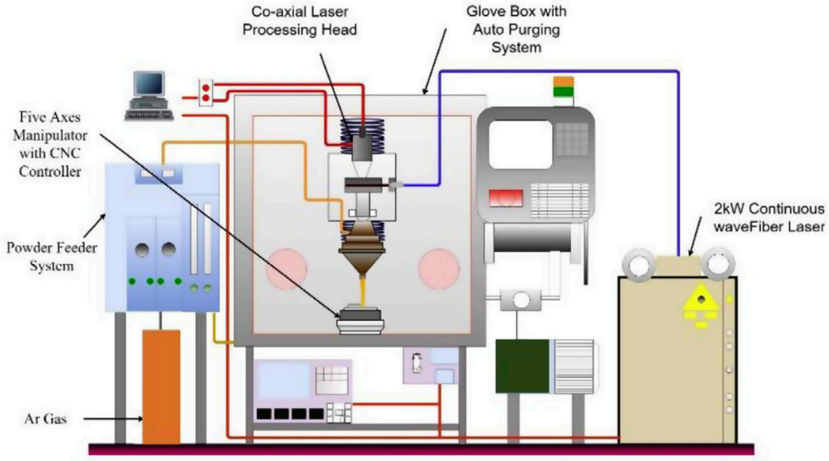

Figure 6. Schematic diagram of the directional energy deposition device. Reprinted with permission from Ref. [74]. Copyright 2019 Elsevier.

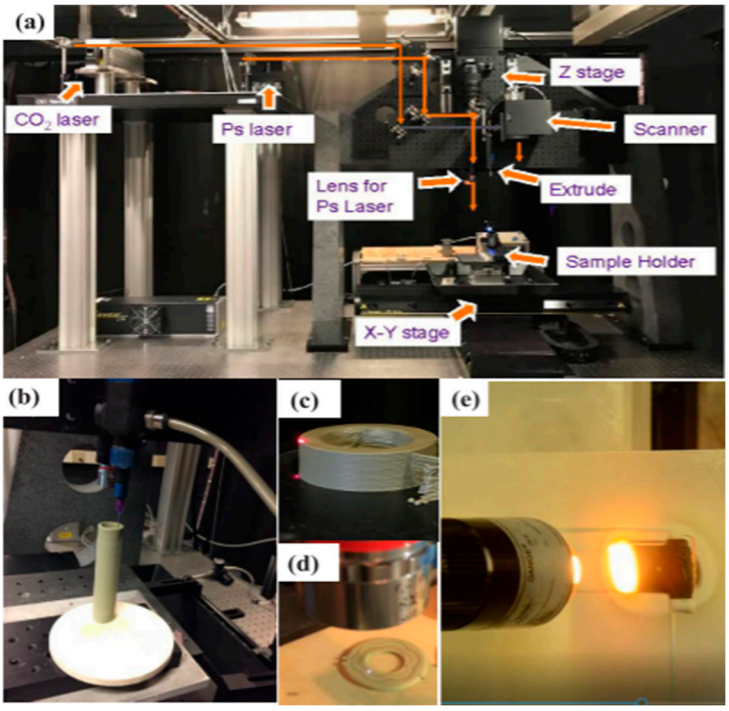

Figure 7. (**a**) Overall framework; (**b**) 3D printing technology; (**c**) CO_2 laser rapid drying; (**d**) Picosecond laser microprocessing; and (**e**) CO_2 laser reaction sintering technology. Reprinted from Ref. [79].

Mu et al. [78], using L3DP, crafted a $BaCe_{0.7}Zr_{0.1}Y_{0.1}Yb_{0.1}O_{3-\delta}$ mixed-conducting membranes. The findings revealed that the mixed-conducting membranes exhibited remarkable integrity and complete densification. Moreover, the grain boundaries of the mixed-conducting membranes were notably reduced, resulting in a proton conductivity of 7×10^{-3} S cm^{-1}.

Direct Ink Writing (DIW), also known as auto-injection molding, is a ceramic 3D printing technology with extremely high efficiency [80]. The operational principle is illustrated in Figure 8. DIW technology is a manufacturing method where flowing ceramic ink is deposited directly onto a substrate through a nozzle to form ceramic film material. In the DIW process, ceramic ink is loaded into a nozzle and expelled in a flowing state, forming liquid or semi-solid ink droplets. Subsequently, by controlling the nozzle's movement path and the ink's ejection speed, the ink is accurately deposited onto the substrate, forming the

desired ceramic film material. The entire process is computer-controlled, ensuring precise printing based on the designed 3D model. DIW technology offers high precision and flexibility in printing ceramic materials, allowing for the fabrication of complex structures and fine features. Its advantages lie in its low manufacturing cost, flexible preparation process, and suitability for various ceramic materials. Through DIW technology, ceramic film materials can be rapidly and efficiently prepared; it is widely applied in fields such as microelectronic devices, sensors, and optical components [55]. Lastly, challenges such as lower precision in shaping and difficulties in slurry preservation still require improvement and resolution in DIW technology [81].

Cannio et al. [82], using DIW technology, successfully fabricated high-density ceramic membranes with asymmetric structures. These ceramic membranes can be utilized for hydrogen separation at temperatures exceeding 600 °C, demonstrating excellent stability. The adoption of asymmetric structural design effectively reduces the thickness of the dense layer, thereby enhancing the gas permeability of the ceramic membrane. Mu et al. [78] utilized DIW technology in combination with laser rapid drying to prepare mixed-conducting membranes with high conductivity.

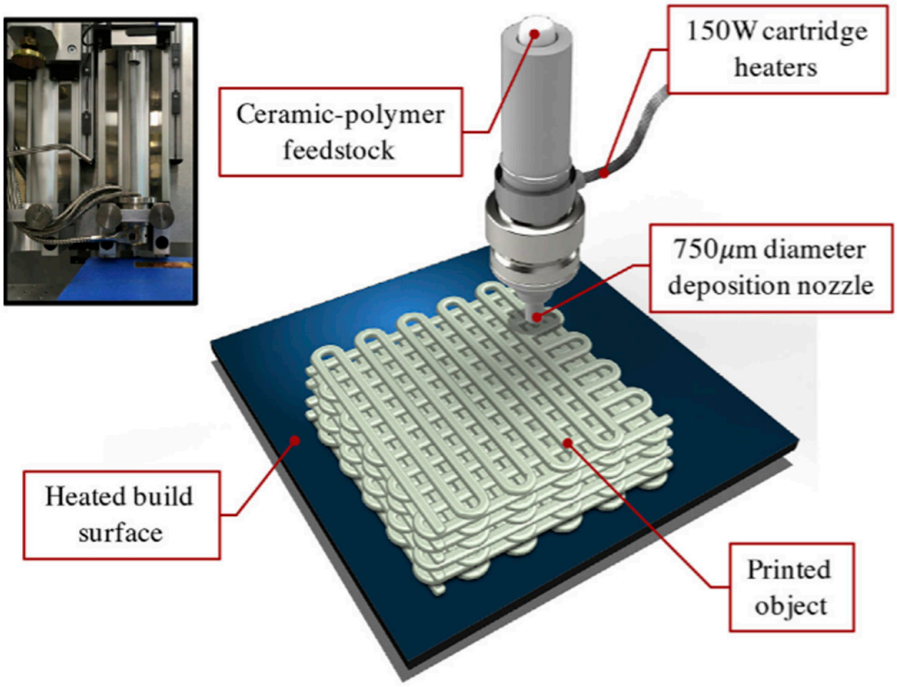

Figure 8. Diagram of a DIW device. Reprinted with permission from Ref. [83] Copyright 2019 Elsevier.

The printing technology of injection molding of ceramic materials is inkjet printing (IJP) technology [84]. Figure 9 shows a schematic diagram of the continuous inkjet printing (CIJ) method. However, unlike the binder jetting (BJ) process, IJP technology is a printing method that utilizes inkjet heads to eject liquid ink or solution onto a substrate to form patterns. This technology is commonly used for the fabrication of flexible electronic devices, organic optoelectronic devices, and other electronic products [85]. In the IJP process, ink is first loaded into the printhead, and then patterns are precisely printed by controlling the movement of the printhead and the position of ink ejection. Compared to traditional printing techniques, IJP offers advantages such as high-speed printing, low cost, suitability for large areas, and flexible substrates. So far, IJP has been applied to solar cells [86,87], sensors [88,89], electronic circuits [90,91], and other fields [69]. Figure 10 illustrates various types of inkjet printers.

He et al. [92] utilized the IJP technique. Ceramic membrane materials with different structures were prepared.

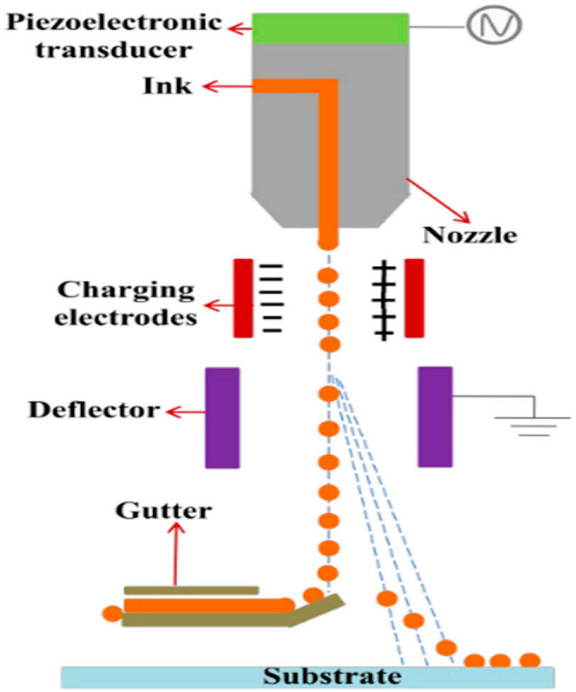

Figure 9. Schematic diagram of the continuous CIJ method. Reprinted with permission from Ref. [93]. Copyright 2019 Materials Chemistry A.

Figure 10. Various types of inkjet printers: (**a**) continuous inkjet printer; (**b**) thermal drop-on-demand (DOD) inkjet printer by Canon; and (**c**) piezoelectric DOD inkjet printer. Reprinted with permission from Ref. [94]. Copyright 2023 Elsevier.

Figure 11 shows the components and working principles of fused deposition modeling (FDM) technology. It shares a similar fabrication process to DIW [95]. The main difference between these two techniques lies in the printing material. The process starts by jetting ceramic powder using high-power lasers or plasma beams. When the melted powder deposits onto the workpiece surface, it rapidly cools and solidifies, forming a thin layer. With each deposition layer, the nozzle deposits new ceramic material onto the workpiece surface based on pre-designed shapes and dimensions. The entire process is computer-controlled, accurately guiding the deposition path based on 3D model data. Deposition can occur in a controlled atmosphere to ensure the quality and stability of the ceramic material. This method is used to manufacture ceramic components with excellent performance and complex geometries, suitable for industries such as aerospace, medical, and energy.

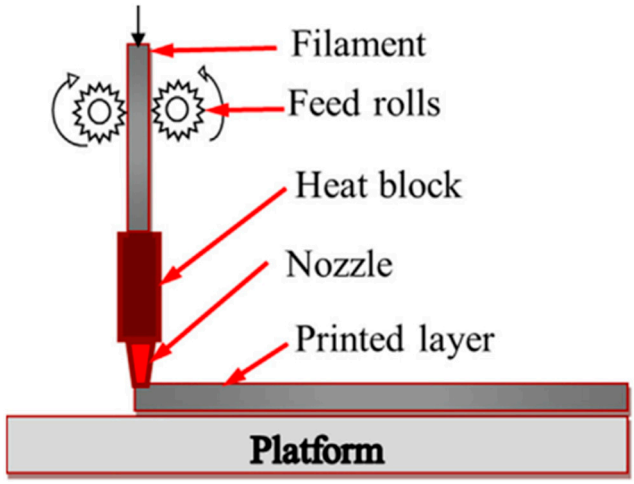

Figure 11. Principle of the FDM process. Reprinted with permission from Ref. [96]. Copyright 2021 Elsevier.

Sheet lamination technology is an additive manufacturing method used to produce three-dimensional objects [97]. Figure 12 illustrates how the laminated object manufacturing technology works. In this process, ceramic powder is first mixed with a polymer aqueous solution or resin to form thin sheets. These sheets are then layered one by one on the printing platform to form a plane. Laser cutting technology is employed to cut each layer of sheet material into the desired shape and size. The cut sheets are then bonded to the printing platform or the previously formed print section using adhesives or heat and cured to ensure stability. As each layer of sheet material is stacked, the printing platform moves downward to provide space for the addition of the next layer of sheets. Laminating technology can combine multiple layers of materials together, significantly enhancing the mechanical strength and durability of the film material. Laminated film materials typically exhibit better dimensional stability and flatness, making them easier for subsequent processing and handling. But, it also suffers from drawbacks: the utilization efficiency of materials is low and the structure between layers is obvious [98].

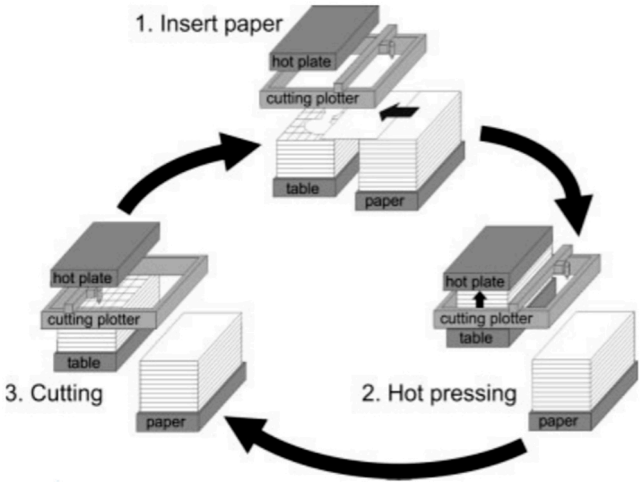

Figure 12. Operating mode of LOM technology. Reprinted with permission from Ref. [99]. Copyright 2004 Wiley.

Aerosol-assisted chemical vapor deposition (AA-CVD) is a method for producing ceramic film materials by generating an aerosol containing ceramic precursor materials and transporting it to a deposition area using a gas carrier. In the deposition area, the aerosol reacts with other gasses in the atmosphere, causing the ceramic precursor material

to deposit on the substrate surface and gradually grow into a thin film. Heat treatment is then applied to enhance the film's crystallinity and mechanical properties. AA-CVD offers the advantages of simplicity and low cost during the manufacturing process, making it highly applicable for various applications. Anna et al. [32] successfully fabricated standalone electrolyte membranes for silicon-based micro-solid oxide fuel cells (SOFCs) using AA-CVD. Due to the gas-phase deposition mechanism, the electrolyte films exhibited moderate tensile stress, resulting in a membrane yield of approximately 90%. Columnar YSZ films and (yttria-stabilized, zirconia/gadolinia-doped ceria) YSZ/GDC films were selected due to their excellent conductivity. Fuel cell testing was conducted using conventional 80 nm sputtered Pt cathodes and anodes. The test results clearly show that the electrolyte resistance drop does not limit its electrochemical performance. It was found that the area's specific resistance is the same as that of the thin YSZ and YSZ/GDC layers.

Physical vapor deposition (PVD) is a method for manufacturing ceramic film materials. The principle involves heating ceramic precursor materials to high temperatures, causing them to evaporate or sublime into a gas, which then deposits onto the surface of a substrate to form a thin film. PVD processes typically include evaporation, sputtering, and laser ablation. In the evaporation method, ceramic materials are heated to their evaporation temperature to form vapor that condenses into a film on the substrate surface. Sputtering involves placing ceramic targets in a vacuum chamber and bombarding them with ion beams or inert gasses to release atoms or molecules, which then deposit onto the substrate to form a film. Laser ablation uses a laser beam to irradiate the surface of ceramic targets, causing them to sublime or evaporate and then deposit onto the substrate to form a film [100,101].

In the Table 2, Compares different advanced manufacturing methods.

Table 2. Comparison of different advanced methods.

Methods	Materials	Applications	Benefits	Drawbacks	Resolution Range (μm)
Fused deposition modeling	Continuous fiber-reinforced polymers	Advanced composite parts	Low cost	Limited material properties	50–200 μm [102]
Powder bed fusion	Compacted fine powders, Ceramics and polymers	Structures, Heat exchangers	High quality	High porosity in the binde	80–250 μm [102]
Inkjet printing and contour crafting	Concrete and soil	Large Structures	Quick printing	Lack of adhesion between layers, Layer-by-layer finish	Inkjet: 5–200 μm [103]
Stereolithography	A resin with photo-active monomers, Hybrid polymer-ceramics	Prototyping	Fine resolution	Expensive	10 μm [102]
Laminated object manufacturing	Metal rolls	Electronics, Smart structures	A vast range of materials	Limitation in manufacturing of complex shapes	Depends on the thickness of the laminates

3. Electrochemical Properties

Mu et al. [104] achieved the successful fabrication of $BaCe_{0.7}Zr_{0.1}Y_{0.1}Yb_{0.1}O_{3-\delta}$+1wt%NiO (BCZYYb+1wt%NiO) and $BaZr_{0.8}Y_{0.2}O_{3-\delta}$+1wt%NiO (BZY20+1wt%NiO) utilizing the rapid laser reactive sintering (RLRS) technique for the first time. The crosssectional image of BCZYYb+1wt%NiO (Figure 13a) vividly reveals a fully dense mixed-conducting membrane. Analysis conducted via Image J on multiple scanning electron microscopy (SEM) images indicates a relative density surpassing 95%. With relatively larger grain sizes, this is poised to notably enhance the overall proton conductivity of the thin films. Figure 13b illustrates that, following the addition of 1wt%NiO sintering aid, the notoriously difficult-to-sinter BZY20+1wt%NiO mixed-conducting membrane is fully densified.

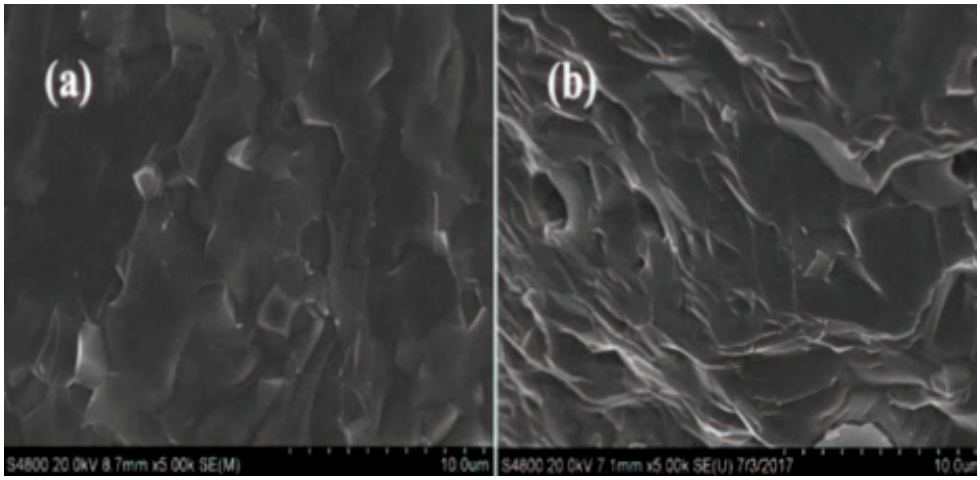

Figure 13. SEM image of a mixed-conducting membranes acquired by RLRS: (**a**) Cross-section of the BCZYYb+1wt%NiO mixed-conducting membranes. (**b**) Cross-section of BZY20+1wt%NiO mixed-conducting membranes. Reprinted from Ref. [104].

In this research endeavor, Mu and the research team ventured into the application of the cutting-edge cathode material $BaCo_{0.4}Fe_{0.4}Zr_{0.1}Y_{0.1}O_{3-\delta}$ (BCFZY0.1) within RLRS half-cell configurations. The primary cells assembled with BCZYYb+1wt%NiO/BCZYYb+60wt% NiO/$BaCo_{0.4}Fe_{0.4}Zr_{0.1}Y_{0.1}O_{3-\delta}$(BCFZY0.1) were tested, subsequently subjecting them to open-circuit voltage assessments to gauge their Ohmic resistance and conductivity. The data in Figure 14 represents the conductivity measurements of a single cell under open-circuit voltage conditions (air/H_2). Figure 14 elucidates the proton conductivity of BCZYYb+1wt% NiO mixed-conducting membranes within the temperature confines of 450 to 650 °C, boasting activation energy of approximately 30 kJ/mol. Leveraging thickness determinations derived from SEM characterizations, the team meticulously computed these parameters. The outcomes underscore the favorable proton conductivity performance exhibited by BCZYYb+1wt%NiO mixed-conducting membranes synthesized via the RLRS technique, showcasing a conductivity of approximately 5.3×10^{-3} S/cm at 600 °C. This serves as a testament to the promising prospects of RLRS methodology within the realm of proton ceramic production.

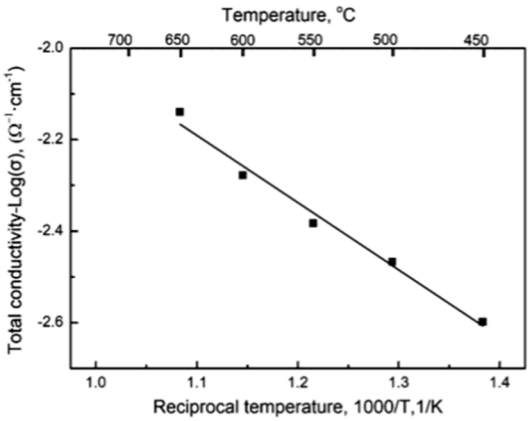

Figure 14. Conductivity of BCZYYb+1wt%NiO mixed-conducting membranes obtained by the RLRS method, measured under open-circuit voltage conditions (air/H_2, no humidification). Reprinted from Ref. [104].

Masciandaro et al. [58], using DLP technology, fabricated corrugated yttria-stabilized zirconia (YSZ) electrolyte membranes through 3D printing. After sintering at 1450 °C, SEM images reveal a densely packed and uniform microstructure, as shown in Figure 15a. Cross-

sectional SEM images of the electrolyte membrane (Figure 15b,c) indicate high density and uniformity, with a thickness of approximately 340 µm. Subsequent electrochemical testing of the assembled single cells using lanthanum strontium manganite (LSM)-YSZ/YSZ/NiO-YSZ demonstrated an ionic conductivity of 0.022 S/cm at 900 °C and an open-circuit voltage of 1.14 ± 0.05 V at 800 °C, aligning with theoretical values and confirming the excellent gas-tightness of the 3D printed membrane. At 900 °C, the peak power density reached 100 mW/cm^2, consistent with the expected values for SOFCs based on dense 3 mol% yttria-stabilized zirconia (3YSZ) electrolytes of the current thickness. Thus, the concept of a 3D-printed electrolyte solid oxide fuel cell has been validated. Similar to flat membranes, honeycomb electrochemical cells were prepared by connecting two electrodes, with NiO-YSZ as the anode and LSM-YSZ as the cathode. The data in Figure 16 depicts conductivity measurements of a single cell conducted in humidified hydrogen gas and synthetic air environments, across various temperatures (T = 800, 850, and 900 °C). Figure 16 presents the V-I polarization curves of the honeycomb cell at 800 °C, 850 °C, and 900 °C. The open-circuit voltage values align with theoretical predictions, confirming the gas-tightness and full density of the DLP-printed electrolyte membranes. At 900 °C, the peak power density of the honeycomb cell reached 115 mW/cm^2, as shown in Figure 17, compared to flat batteries. The data in Figure 17 show the EIS spectrum of individual cells measured at V = 0.7 V.

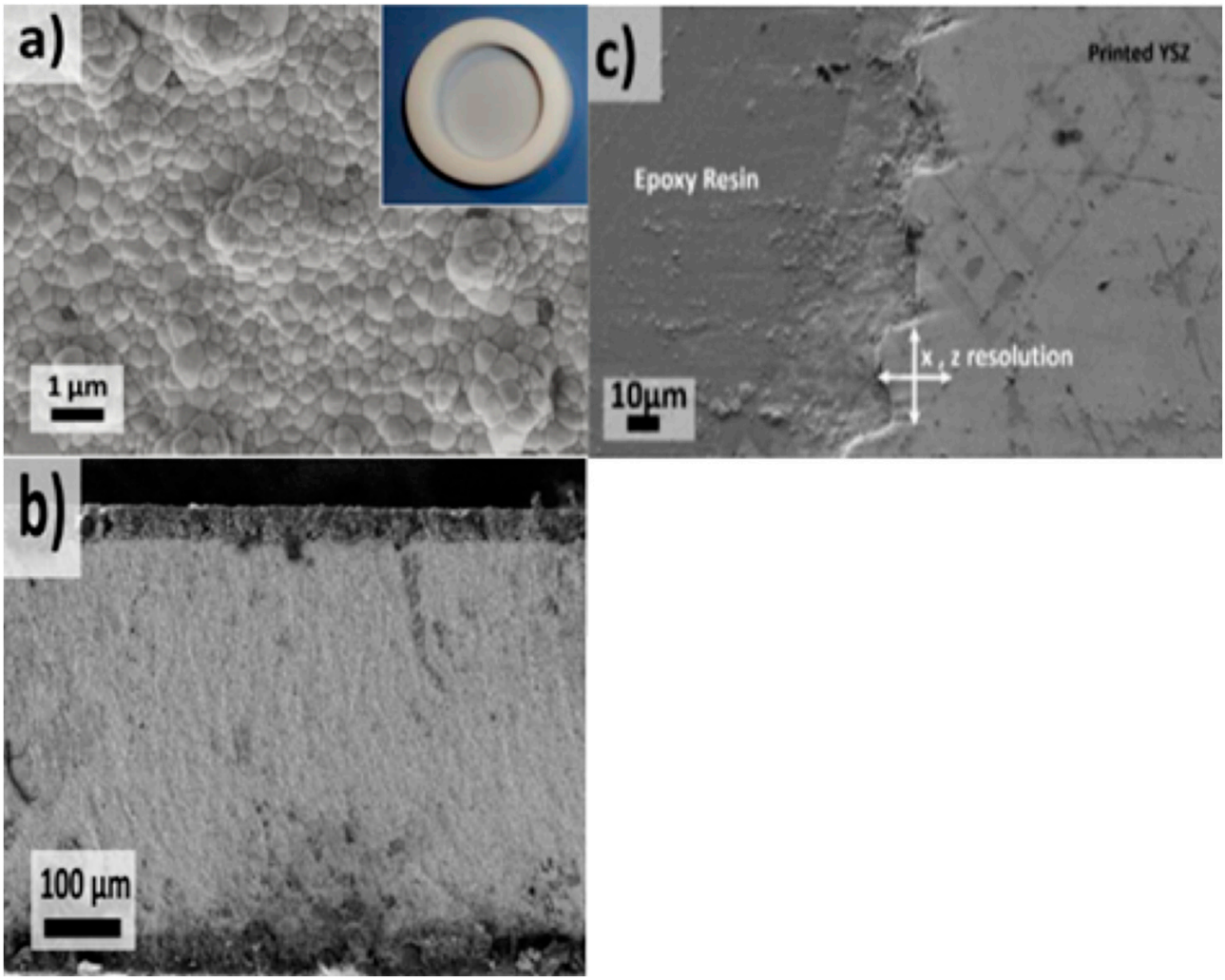

Figure 15. (**a**) SEM image of 3YSZ electrolyte. SEM images of the cross-section of the self-supporting membrane showing (**b**) electrodes on both sides and (**c**) high resolution and density. Reprinted with permission from Ref. [58]. Copyright 2019 Elsevier.

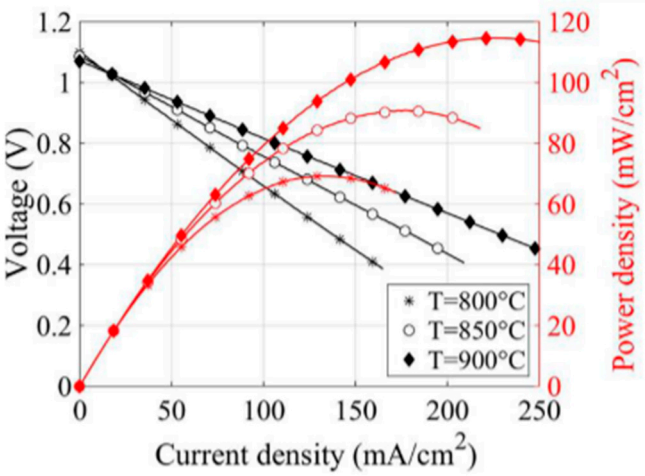

Figure 16. Voltage and power-current density curves of a honeycomb-shaped ceramic electrolyte fuel cell (Ni-YSZ/YSZ/YSZ-LSM) operating under humidified hydrogen and synthetic air and at different temperatures (T = 800, 850, 900 °C). Reprinted with permission from Ref. [58]. Copyright 2019 Elsevier.

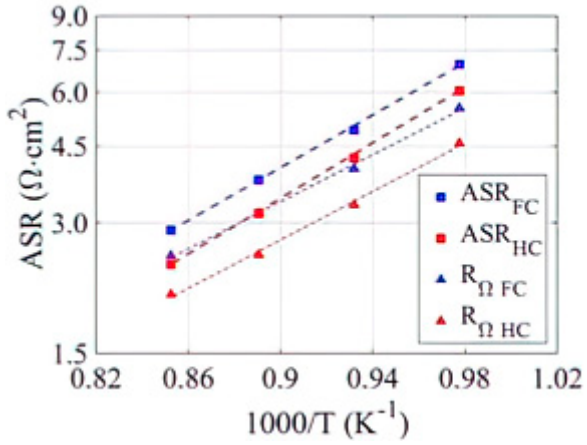

Figure 17. The ohmic ratio resistance and the total area ratio resistance as a function of the reciprocal temperature of the planar and honeycomb-shaped electrolytes were obtained by electrochemical impedance spectroscopy (EIS) measured at V = 0.7 V. Reprinted with permission from Ref. [58]. Copyright 2019 Elsevier.

Arianna et al. [59], utilizing DLP technology, fabricated planar and corrugated lanthanum strontium manganite/yttria-stabilized zirconia (LSM-YSZ)/YSZ/Ni-YSZ fuel cells. Figure 18 presents cross-sectional SEM images of the different layers and interfaces of both planar and corrugated cells. It is evident from Figure 18e,f that the cells exhibit defect-free and homogeneous layers, with densities exceeding 97% of the theoretical value. The data in Figures 19 and 20 were obtained by connecting the electrical output to a potentiostat and frequency response analyzer instrument, allowing for the study of V-I curves. Figures 19 and 20 display the V-j curves measured at 900 °C for both cells. The open-circuit voltages (OCVs) for both cells are close to 1.10 V, aligning well with the expected values estimated by the Nernst equation, thereby confirming the gas-tightness and high quality of the planar and corrugated electrolytes. At 900 °C, the planar cell achieved a peak power density of 260 mW cm^{-2}, which is higher than similar cells produced by traditional methods. Meanwhile, the corrugated cell exhibited a peak power density of 410 mW cm^{-2}, significantly surpassing that of the planar cell. The increase in peak power density is attributed to the enhanced active area of the corrugated cell.

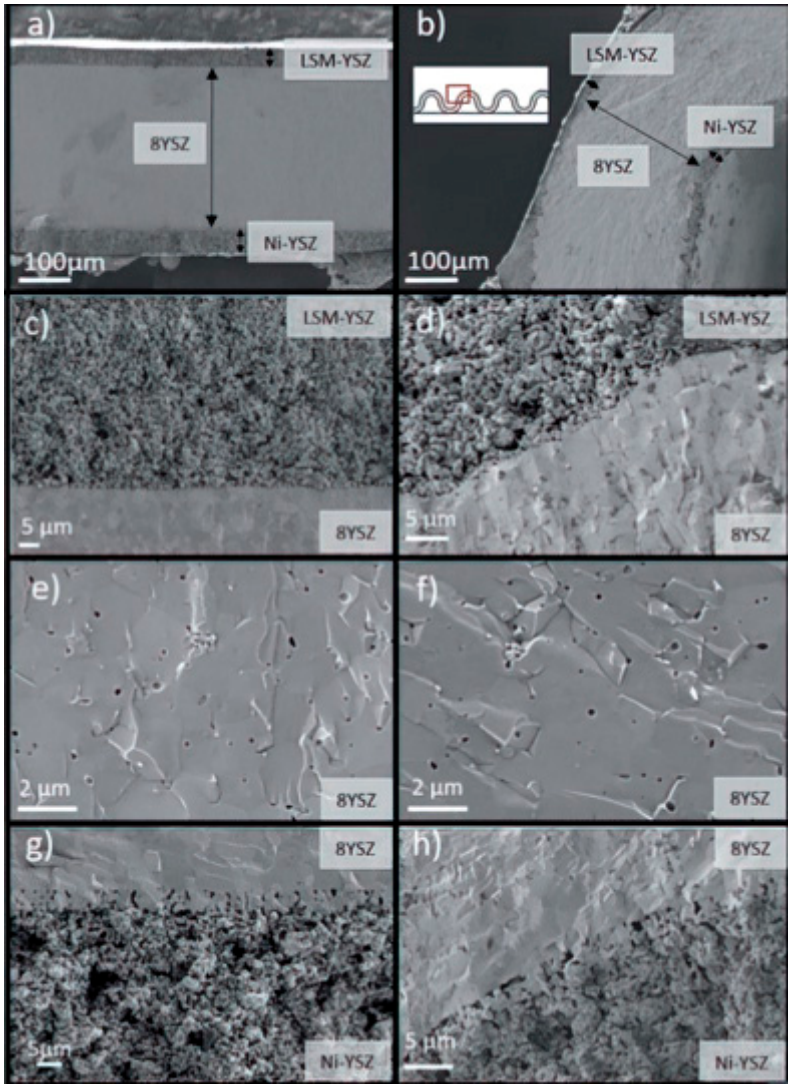

Figure 18. Cross-section SEM images of the planar (**a**,**c**,**e**,**g**) and corrugated (**b**,**d**,**f**,**h**) cells. Reprinted from Ref. [59].

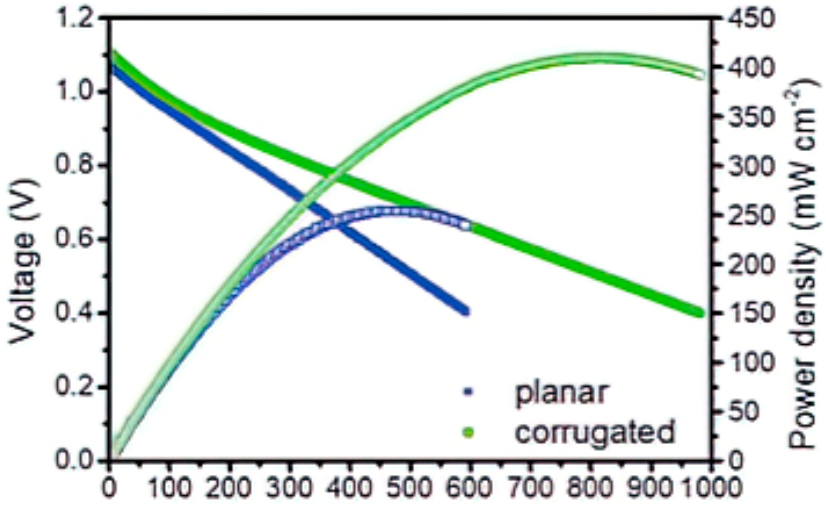

Figure 19. V-j curves of planar cells measured with fuel cells at 900 °C. Reprinted from Ref. [59].

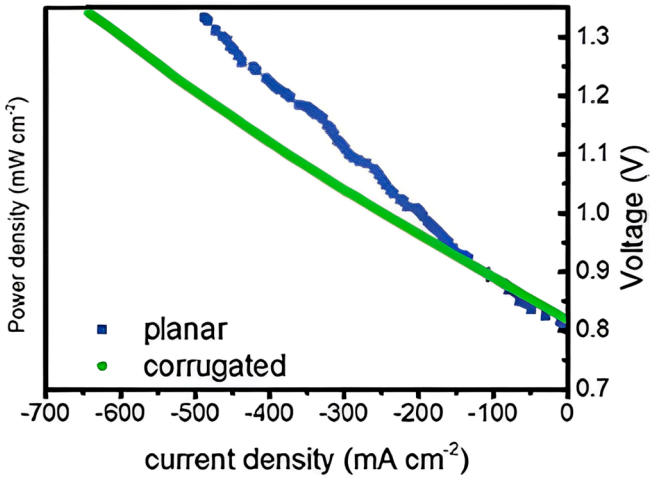

Figure 20. The V-j curve of the corrugated cell was measured in co-electrolysis mode at 900 °C. Reprinted from Ref. [59].

Xing et al. [70], in pursuit of high-performance solid oxide fuel cells (SOFCs), fabricated dense 8 mol% yttria-stabilized zirconia (8YSZ) ceramic electrolyte membranes and their supported 8YSZ fuel cells using DLP 3D printing technology. The data in Figures 21 and 22 were obtained using a solid oxide fuel cell testing system, where the EIS of planar electrolyte and planar full cells was measured over a frequency range of 0.1 Hz to 10 kHz. Figure 21 illustrates Nyquist plots of sintered 8YSZ samples at different temperatures, confirming the gas-tightness of the electrolyte membranes at 800 °C. The decrease in the conductivity of the sintered sample at 1500 °C is due to the increase in grain size. Meanwhile, the conductivity of samples sintered at 1400 and 1450 °C remains within a reasonable range. Figure 22 displays I-V-P curves of the cells at temperatures of 700 and 800°C, respectively. At a temperature of 800 °C, the full cell power density is 114.3 mW cm^{-2}, which is lower compared to electrolytes of similar thickness. This lower performance may be due to detachment between the cathode layer and the electrolyte layer, along with smaller electrode pores, resulting in reduced power density. These results demonstrate the feasibility of constructing self-supporting SOFC electrolytes with the desired structure using 3D printing technology.

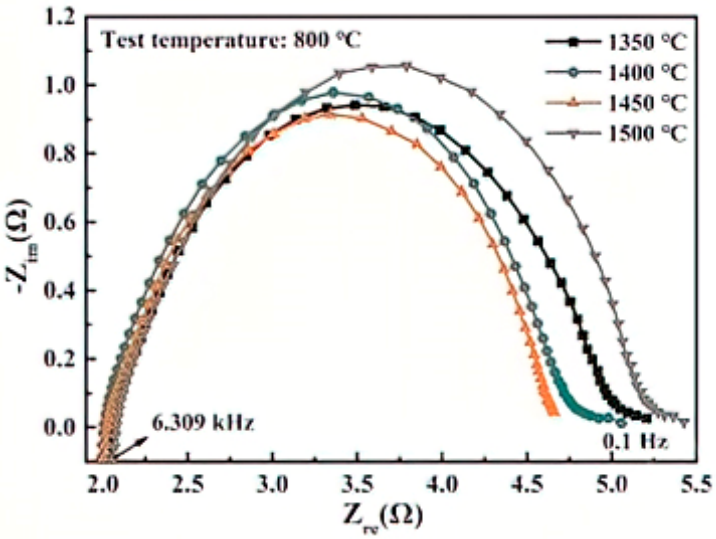

Figure 21. EIS of 8YSZ ceramics sintered at different temperatures. Reprinted with permission from Ref. [70]. Copyright 2020 Elsevier.

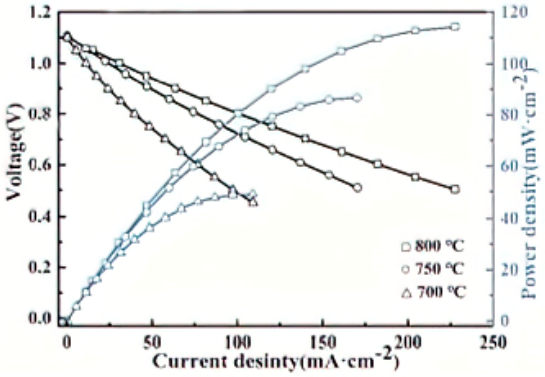

Figure 22. Electrochemical performance of the fuel cell operated at different temperatures. Reprinted with permission from Ref. [70]. Copyright 2020 Elsevier.

Mu et al. [78], using the RLRS technique, welded a mixed-conducting membranes $BaCe_{0.7}Zr_{0.1}Y_{0.1}Yb_{0.1}O_{3-\delta}$+1wt%NiO (BCZYYb+1wt%NiO) onto a pre-sintered Ni(O)+BCZYYb anode substrate. From high-magnification SEM images (Figure 23a), it can be observed that the mixed-conducting membrane surface is defect-free and densified. Further confirmation of the fully dense, mixed-conducting membranes derived from RLRS with BCZYYb+1wt%NiO is shown in the SEM cross-sectional image (Figure 23b). Subsequently, primary cells assembled with Ni-BCZYYb/BCZYYb+1wt%NiO/BCFZY0.1 ($BaCo_{0.4}Fe_{0.4}Zr_{0.1}Y_{0.1}O_{3-\delta}$) were tested. Measurement methodology for the data in Figure 24: Firstly, the single cell was heated at a rate of 1 °C/min to 100 °C and held for 1 h, followed by heating at 1 °C/min to 300 °C and holding for 1 h. Subsequently, the single cell was heated at a rate of 1.5 °C/min to 600 °C. During the heating process, the anode and cathode were exposed to stagnant air. Initially, 5% H_2 was injected into the anode at a rate of 20 mL/min for the first 6 h and then switched to pure hydrogen for measurement. Air was swept through the cathode at a rate of 150 mL/min. The I-V characteristics were corrected at different temperatures using a potentiostat. Figure 24 presents the I-P-V curves of the single cells, with OCVs of 0.97 V at 600 °C and 0.94 V at 650 °C, consistent with measured values. Additionally, Figure 24 shows that the peak power densities of the single cells after RLRS were 97 mW cm^{-2} at 600 °C and 121 mW cm^{-2} at 650 °C, which are lower than those achieved by state-of-the-art protonic ceramic fuel cell (PCFC) single cells. In addition, the proton conductivity of BCZYYb+1wt%NiO films after RLRS is 3.7×10^{-3} S cm^{-1} at 600 °C. Further optimization of the film thickness, composition, and microstructure is expected to enhance PCFC performance.

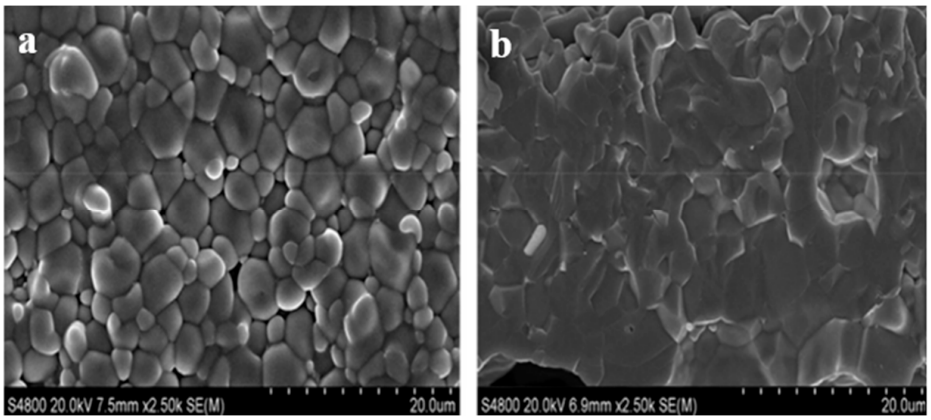

Figure 23. (**a**) High-power surface photograph of BCZYYb+1wt%NiO after RLRS. (**b**) High-power cross-section of BCZYYb+1wt%NiO mixed-conducting membranes after RLRS photo. Reprinted from Ref. [78].

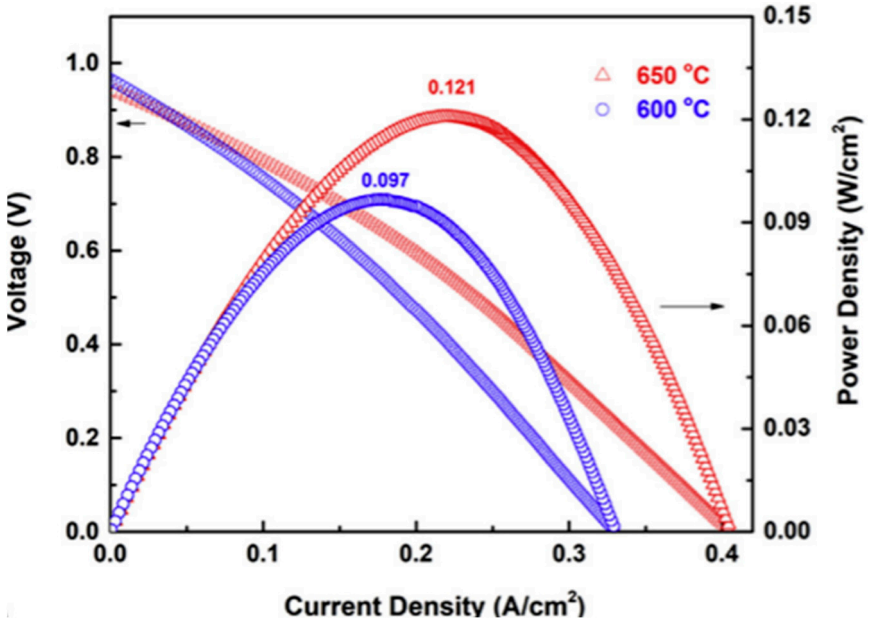

Figure 24. I-V-P curves of Ni-BCZYYb/BCZYYb+1wt%NiO/BCFZY0.1 single cells. Reprinted from Ref. [78].

In addition to this, we have summarized the electrochemical properties of SOFCs prepared by different advanced methods, as shown in Table 3.

Table 3. Comparison of different preparation methods for SOFC performance. (NCAL = $Ni_{0.8}Co_{0.15}Al_{0.05}LiO_{2-\delta}$, SSC = $Sm_{0.5}Sr_{0.5}CoO_3$, SDC = $Sm_{0.2}Ce_{0.8}O_{1.9}$, GDC = $Ce_{0.8}Gd_{0.2}O_{1.9}$, LSM[1] = $La_{0.9}Sr_{0.1}MnO_3$, LSM[2] = $La_{0.8}Sr_{0.2}MnO_3$, $BaCe_{0.7}Zr_{0.1}Y_{0.1}Yb_{0.1}O_{3-\delta}$ = BCZYYb, BCFZY0.1 = $BaCo_{0.4}Fe_{0.4}Zr_{0.1}Y_{0.1}O_{3-\delta}$, and Selective laser sintering = SLS.

Printed Electrolyte	Preparation Method	SOFC Component	Operating Temperature (°C)	Peak Power Density (W cm^{-2})	Open Circuit Voltage (V)	Reference
YSZ	IJP	NiO-YSZ/ YSZ/YSZ/ LSM[1]-YSZ	800	1.50	1.09	[105]
SDC	DIW	NCAL/SDC-SSC/NCAL	550	0.44	1.00	[106]
YSZ	DLP-SLS	Ag-GDC/ YSZ/Ag-GDC	850	0.17	1.04	[107]
YSZ	DLP	NiO-YSZ/YSZ/LSM[2]	800	0.11		[70]
BCZYYb	RLRS	Ni(O)+BCZYYb/BCZYYb+ 1wt%NiO/BCFZY0.1	600	0.097	0.96	[78]

Qi et al. [108] developed an electrochemical ceramic membrane bioreactor (ECMBR) for pollutant removal. The electrochemical ceramic membrane module was constructed as follows: A titanium mesh was vertically fixed in the center of a polyvinyl chloride (PVC) frame to serve as the cathode, with the Ti/SnO_2-Sb-La cathode fixed on both sides of this framework. The Ti/SnO_2-Sb-La was prepared via the sol–gel method, and the anode and cathode were connected using titanium wire, with a direct current power supply applied. Finally, the anode was affixed to the PVC frame using an epoxy resin adhesive, completing the assembly of the electrochemical ceramic membrane module. The results demonstrate that, under an electric field of 2 V/cm, the ECMBR significantly enhanced the removal efficiency of most target pollutants without adversely affecting the removal of other pollutants or causing additional membrane fouling. Furthermore, the electric field did not alter the microbial community, suggesting that the increase in pharmaceutical and

personal care products(PPCP) removal was mainly due to electrochemical oxidation within the ECMBR.

Zheng et al. [109] developed an electrochemical cell with a Ti/SnO_2-Sb anode and an electrochemically porous ceramic membrane; an electrochemical reactor was employed to study the degradation of p-chloroaniline (PCA) under specific current conditions. The results revealed that when a current of 0.8 A was applied, with a membrane flux of 80 Lm^{-2} h^{-1}, and 0.2 mM Fe^{2+} was added at pH 3, PCA was completely degraded after 90 min of electrolysis. The mineralization rate reached 75.1%, and the total nitrogen removal was 46.7%.

4. Advanced Preparation Process Improves the Performance of Ceramic Electrolyte Membranes

The advanced preparation method can accurately control the composition, microstructure, and morphology of the ceramic membrane; improve the compactness, hardness, corrosion resistance, and high temperature stability of the membrane material; and meet the requirements of different application fields for the performance of the ceramic membrane. These methods can also achieve uniformity and thickness control of the film, improving the functionality and application performance of the ceramic film. For instance, in the field of ceramic fuel cells, 3D printing technologies can be employed to construct ceramic electrolyte membranes with corrugated structures, resulting in a surface area increase of over 35% compared to flat ceramic membranes [59,70,71]. In solid oxide fuel cells (SOFCs), the utilization of such corrugated, structured, dense ceramic membranes can significantly enhance the overall mechanical performance [58,110]. Bae et al. [111], using the pulsed laser deposition (PLD) technique, successfully fabricated an approximately 1.5 μm thick $BaCe_{0.55}Zr_{0.3}Y_{0.15}O_{3-\delta}$ (BCZY) film on anode-supported single cells. These cells achieved an ultra-low ohmic resistance of 0.15 Ω cm^2, proportional to the electrolyte thickness, with an open circuit voltage (OCV) of 1.03 V and a maximum power density of 500 mW cm^{-2} at 600 °C.

In summary, these advanced preparation methods have not only enhanced the structural control capabilities and physicochemical properties of ceramic membrane materials, but have also significantly bolstered their performance in practical applications such as fuel cells, electrolyzers, and supercapacitors, meeting the demands for high performance and reliability [112–114]. Additionally, ceramic membranes play a crucial role in electrochemical sensors and catalysis, due to their high stability and tunable pore structures, which enable them to maintain performance in demanding chemical environments while providing efficient catalytic activity [6,115]. These methods have comprehensively optimized the electrical conductivity, mechanical strength, and electrochemical reaction efficiency of ceramic membrane materials, thereby advancing the field of electrochemical applications.

5. Future Directions

In the field of electrochemistry, the structure of ceramic membrane materials is crucial for their performance. These membranes should exhibit high porosity and a uniform pore size distribution to enhance permeability. Additionally, maintaining good thermal stability and chemical compatibility ensures that the materials are compatible with electrolytes and other chemicals in the environment. Ceramic membranes also require good ionic or electronic conductivity. Therefore, it is evident that the structure of ceramic membranes directly determines their performance, making manufacturing technology a critical factor in their performance.

Currently, there are many methods for preparing ceramic membranes, but many of these methods lack the capability to produce complex ceramic membrane structures, limiting the development of ceramic-membrane-based electrochemical devices in electrochemical applications. Hence, there is a need to develop new technologies for manufacturing membrane materials that meet low-cost and more complex structure requirements, thereby producing high-performance electrochemical devices.

Author Contributions: Writing—original draft preparation, K.F.; writing—review and editing, M.Y.; conceptualization, writing—review and editing, and supervision, M.Y., J.L. and S.M. All authors have read and agreed to the published version of the manuscript.

Funding: This research was funded by the Youth Fund of the National Natural Science Foundation of China for the investigation of picosecond laser micro-machining-assisted in situ 3D printing rapid laser reactive sintering for the fabrication of high performance protonic ceramic fuel cell stacks (52202271); the Provincial Doctoral Research Start-up Fund Project from Liaoning Provincial Department of Science and Technology for the study of fabrication technology on protonic ceramic-based fuel cell by laser 3D printing (2023-BS-144); the Liaoning Provincial Department of Education youth project for the study of the creation and functionalization of low-temperature, colored aeolian sand (JYTQN2023375); Shenyang University of Chemical Technology "Excellent Youth" Support Project (2023YQ001).

Data Availability Statement: No new data were created or analyzed in this study. Data sharing is not applicable to this article

Conflicts of Interest: The authors declare no conflicts of interest.

References

1. Fu, W.; Wang, X.; Zheng, J.; Liu, M.; Wang, Z. Antifouling performance and mechanisms in an electrochemical ceramic membrane reactor for wastewater treatment. *J. Membr. Sci.* **2019**, *570*, 355–361. [CrossRef]
2. Heddrich, M.P.; Gupta, S.; Santhanam, S. Electrochemical ceramic membrane reactors in future energy and chemical process engineering. *Chem. Ing. Tech.* **2019**, *91*, 809–820. [CrossRef]
3. Ahmad Kamaroddin, M.F.; Sabli, N.; Tuan Abdullah, T.A.; Siajam, S.I.; Abdullah, L.C.; Abdul Jalil, A.; Ahmad, A. Membrane-based electrolysis for hydrogen production: A review. *Membranes* **2021**, *11*, 810. [CrossRef] [PubMed]
4. Herradon, C.; Le, L.; Meisel, C.; Huang, J.; Chmura, C.; Kim, Y.; Cadigan, C.; O'Hayre, R.; Sullivan, N. Proton-conducting ceramics for water electrolysis and hydrogen production at elevated pressure. *Front. Energy Res.* **2022**, *10*, 1020960. [CrossRef]
5. Fedotov, A.; Tsodikov, M.; Yaroslavtsev, A. Hydrogen production in catalytic membrane reactors based on porous ceramic converters. *Processes* **2022**, *10*, 2060. [CrossRef]
6. Chen, M.; Zheng, J.; Dai, R.; Wu, Z.; Wang, Z. Preferential removal of 2, 4-dichlorophenoxyacetic acid from contaminated waters using an electrocatalytic ceramic membrane filtration system: Mechanisms and implications. *Chem. Eng. J.* **2020**, *387*, 124132. [CrossRef]
7. Ren, L.; Ma, J.; Chen, M.; Qiao, Y.; Dai, R.; Li, X.; Wang, Z. Recent advances in electrocatalytic membrane for the removal of micropollutants from water and wastewater. *Iscience* **2022**, *25*, 104342. [CrossRef] [PubMed]
8. Dong, X.; Jin, W.; Xu, N.; Li, K. Dense ceramic catalytic membranes and membrane reactors for energy and environmental applications. *Chem. Commun.* **2011**, *47*, 10886–10902. [CrossRef] [PubMed]
9. Gu, Q.; Ng, T.C.A.; Bao, Y.; Ng, H.Y.; Tan, S.C.; Wang, J. Developing better ceramic membranes for water and wastewater Treatment: Where microstructure integrates with chemistry and functionalities. *Chem. Eng. J.* **2022**, *428*, 130456. [CrossRef]
10. Linkov, V.; Petrik, L.; Vaivars, G.; Maluleke, A.; Gericke, G. Ceramic-based materials for electrochemical applications. *Proc. Macromol. Symp.* **2002**, *178*, 153–168. [CrossRef]
11. Minh, N.Q. Ceramic fuel cells. *J. Am. Ceram. Soc.* **1993**, *76*, 563–588. [CrossRef]
12. Wang, Y.; Leung, D.Y.; Xuan, J.; Wang, H. A review on unitized regenerative fuel cell technologies, part-A: Unitized regenerative proton exchange membrane fuel cells. *Renew. Sustain. Energy Rev.* **2016**, *65*, 961–977. [CrossRef]
13. Xia, C.; Liu, M. A simple and cost-effective approach to fabrication of dense ceramic membranes on porous substrates. *J. Am. Ceram. Soc.* **2001**, *84*, 1903–1905. [CrossRef]
14. Saridag, S.; Tak, O.; Alniacik, G. Basic properties and types of zirconia: An overview. *World J. Stomatol.* **2013**, *2*, 40–47. [CrossRef]
15. Bragg, W.; Gottfried, C.; West, J. The structure of β alumina. *Z. Krist.-Cryst. Mater.* **1931**, *77*, 255–274. [CrossRef]
16. Duwez, P.; Odell, F.; Brown, F.H., Jr. Stabilization of zirconia with calcia and magnesia. *J. Am. Ceram. Soc.* **1952**, *35*, 107–113. [CrossRef]
17. Meulenberg, W.A.; Schulze-Küppers, F.; Deibert, W.; Gestel, T.V.; Baumann, S. Ceramic membranes: Materials–components–potential applications. *ChemBioEng Rev.* **2019**, *6*, 198–208. [CrossRef]
18. Ghosh, D.; Sinha, M.; Purkait, M. A comparative analysis of low-cost ceramic membrane preparation for effective fluoride removal using hybrid technique. *Desalination* **2013**, *327*, 2–13. [CrossRef]
19. Del Colle, R.; Fortulan, C.A.; Fontes, S.R. Manufacture and characterization of ultra and microfiltration ceramic membranes by isostatic pressing. *Ceram. Int.* **2011**, *37*, 1161–1168. [CrossRef]
20. Liang, D.; Huang, J.; Zhang, H.; Fu, H.; Zhang, Y.; Chen, H. Influencing factors on the performance of tubular ceramic membrane supports prepared by extrusion. *Ceram. Int.* **2021**, *47*, 10464–10477. [CrossRef]
21. Li, X.; Wei, J.; Chen, B.; Wang, Y.; Jiang, C.; Zhang, H.; Qiao, M. Effective electromagnetic wave absorption and photoluminescence performances of flexible SiC nanowires membrane. *Ceram. Int.* **2021**, *47*, 17615–17626. [CrossRef]

22. Chen, X.; Zou, D.; Lin, Y.; Zhang, W.; Qiu, M.; Fan, Y. Enhanced performance arising from low-temperature preparation of α-alumina membranes via titania doping assisted sol-gel method. *J. Membr. Sci.* **2018**, *559*, 19–27. [CrossRef]
23. Zhu, W.; Liu, Y.; Guan, K.; Peng, C.; Wu, J. Design and optimization of ceramic membrane structure: From the perspective of flux matching between support and membrane. *Ceram. Int.* **2021**, *47*, 12357–12365. [CrossRef]
24. Souza, D.F.; Nunes, E.H.; Queiroga, J.A.; Vasconcelos, W.L. Microstructural characterization and gas permeation performance of freeze-cast alumina supports. *J. Eur. Ceram. Soc.* **2018**, *38*, 4020–4025. [CrossRef]
25. Lee, J.-Y.; An, J.; Chua, C.K. Fundamentals and applications of 3D printing for novel materials. *Appl. Mater. Today* **2017**, *7*, 120–133. [CrossRef]
26. Li, J.; Pumera, M. 3D printing of functional microrobots. *Chem. Soc. Rev.* **2021**, *50*, 2794–2838. [CrossRef]
27. Jiménez, M.; Romero, L.; Domínguez, I.A.; Espinosa, M.d.M.; Domínguez, M. Additive manufacturing technologies: An overview about 3D printing methods and future prospects. *Complexity* **2019**, *2019*, 9656938. [CrossRef]
28. Zhu, J.; Wu, P.; Chao, Y.; Yu, J.; Zhu, W.; Liu, Z.; Xu, C. Recent advances in 3D printing for catalytic applications. *Chem. Eng. J.* **2022**, *433*, 134341. [CrossRef]
29. Karakurt, I.; Lin, L. 3D printing technologies: Techniques, materials, and post-processing. *Curr. Opin. Chem. Eng.* **2020**, *28*, 134–143. [CrossRef]
30. Hwa, L.C.; Rajoo, S.; Noor, A.M.; Ahmad, N.; Uday, M. Recent advances in 3D printing of porous ceramics: A review. *Curr. Opin. Solid State Mater. Sci.* **2017**, *21*, 323–347. [CrossRef]
31. Scheithauer, U.; Kerber, F.; Füssel, A.; Holtzhausen, S.; Beckert, W.; Schwarzer, E.; Weingarten, S.; Michaelis, A. Alternative process routes to manufacture porous ceramics—Opportunities and challenges. *Materials* **2019**, *12*, 663. [CrossRef] [PubMed]
32. Schlupp, M.V.; Evans, A.; Martynczuk, J.; Prestat, M. Micro-Solid Oxide Fuel Cell Membranes Prepared by Aerosol-Assisted Chemical Vapor Deposition. *Adv. Energy Mater.* **2014**, *4*, 1301383. [CrossRef]
33. Liang, F.; Yang, J.; Zhao, Y.; Zhou, Y.; Yan, Z.; He, J.; Yuan, Q.; Wu, J.; Liu, P.; Zhong, Z. A review of thin film electrolytes fabricated by physical vapor deposition for solid oxide fuel cells. *Int. J. Hydrogen Energy* **2022**, *47*, 36926–36952. [CrossRef]
34. Zhang, Y.; Tan, Y.; Sun, R.; Zhang, W. Preparation of ceramic membranes and their application in wastewater and water treatment. *Water* **2023**, *15*, 3344. [CrossRef]
35. Amin, S.K.; Roushdy, M.H.; El-Sherbiny, C.A. An overview of production and development of ceramic membranes. *Chem. Eng.* **2016**, *11*, 7708–7721.
36. Nunes, S.P.; Culfaz-Emecen, P.Z.; Ramon, G.Z.; Visser, T.; Koops, G.H.; Jin, W.; Ulbricht, M. Thinking the future of membranes: Perspectives for advanced and new membrane materials and manufacturing processes. *J. Membr. Sci.* **2020**, *598*, 117761. [CrossRef]
37. Malik, N.; Bulasara, V.K.; Basu, S. Preparation of novel porous ceramic microfiltration membranes from fly ash, kaolin and dolomite mixtures. *Ceram. Int.* **2020**, *46*, 6889–6898. [CrossRef]
38. Son, D.-J.; Kim, W.-Y.; Yun, C.-Y.; Kim, D.-G.; Chang, D.; Sunwoo, Y.; Hong, K.-H. Application of tube-type ceramic microfiltration membrane for post-treatment of effluent from biological wastewater treatment process using phase separation. *Environ. Eng. Res.* **2017**, *22*, 377–383. [CrossRef]
39. Kumar, R.V.; Ghoshal, A.K.; Pugazhenthi, G. Elaboration of novel tubular ceramic membrane from inexpensive raw materials by extrusion method and its performance in microfiltration of synthetic oily wastewater treatment. *J. Membr. Sci.* **2015**, *490*, 92–102. [CrossRef]
40. Yanu, C.A.; Sieliechi, J.M.; Ngassoum, M.B. Optimization of ceramic paste viscosity use for the elaboration of tubular membrane support by extrusion and its application. *J. Mater. Sci. Chem. Eng.* **2020**, *8*, 1–22. [CrossRef]
41. Suresh, K.; Katara, N. Design and development of circular ceramic membrane for wastewater treatment. *Mater. Today Proc.* **2021**, *43*, 2176–2181. [CrossRef]
42. Meghnani, R.; Kumar, M.; Pugazhenthi, G.; Dhakshinamoorthy, V. Synthesis of ceramic membrane using inexpensive precursors and evaluation of its biocompatibility for hemofiltration application. *Sep. Purif. Technol.* **2021**, *256*, 117814. [CrossRef]
43. Abdullah, N.; Rahman, M.A.; Othman, M.H.D.; Ismail, A.; Jaafar, J.; Abd Aziz, A. Preparation and characterization of self-cleaning alumina hollow fiber membrane using the phase inversion and sintering technique. *Ceram. Int.* **2016**, *42*, 12312–12322. [CrossRef]
44. Zhu, Z.; Xiao, J.; He, W.; Wang, T.; Wei, Z.; Dong, Y. A phase-inversion casting process for preparation of tubular porous alumina ceramic membranes. *J. Eur. Ceram. Soc.* **2015**, *35*, 3187–3194. [CrossRef]
45. Choi, M.-B.; Lim, D.-K.; Jeon, S.-Y.; Kim, H.-S.; Song, S.-J. Oxygen permeation properties of BSCF5582 tubular membrane fabricated by the slip casting method. *Ceram. Int.* **2012**, *38*, 1867–1872. [CrossRef]
46. Tsetsekou, A.; Agrafiotis, C.; Milias, A. Optimization of the rheological properties of alumina slurries for ceramic processing applications Part I: Slip-casting. *J. Eur. Ceram. Soc.* **2001**, *21*, 363–373. [CrossRef]
47. Song, J.-H.; Park, S.-I.; Lee, J.-H.; Kim, H.-S. Fabrication characteristics of an anode-supported thin-film electrolyte fabricated by the tape casting method for IT-SOFC. *J. Mater. Process. Technol.* **2008**, *198*, 414–418. [CrossRef]
48. Jabbari, M.; Bulatova, R.; Tok, A.; Bahl, C.; Mitsoulis, E.; Hattel, J.H. Ceramic tape casting: A review of current methods and trends with emphasis on rheological behaviour and flow analysis. *Mater. Sci. Eng. B* **2016**, *212*, 39–61. [CrossRef]
49. Das, N.; Maiti, H.S. Ceramic membrane by tape casting and sol–gel coating for microfiltration and ultrafiltration application. *J. Phys. Chem. Solids* **2009**, *70*, 1395–1400. [CrossRef]
50. Sinha Ray, S.; Lee, H.-K.; Kwon, Y.-N. Review on blueprint of designing anti-wetting polymeric membrane surfaces for enhanced membrane distillation performance. *Polymers* **2019**, *12*, 23. [CrossRef]

51. Ray, S.S.; Deb, C.K.; Chang, H.M.; Chen, S.S.; Ganesapillai, M. Crosslinked PVDF-HFP-based hydrophobic membranes incorporated with CNF for enhanced stability and permeability in membrane distillation. *J. Appl. Polym. Sci.* **2019**, *136*, 48021. [CrossRef]
52. Jun, M.-S.; Choi, Y.-W.; Kim, J.-D. Solvent casting effects of sulfonated poly (ether ether ketone) for Polymer electrolyte membrane fuel cell. *J. Membr. Sci.* **2012**, *396*, 32–37. [CrossRef]
53. Ray, S.S.; Chen, S.-S.; Li, C.-W.; Nguyen, N.C.; Nguyen, H.T. A comprehensive review: Electrospinning technique for fabrication and surface modification of membranes for water treatment application. *RSC Adv.* **2016**, *6*, 85495–85514. [CrossRef]
54. Huang, L.; Manickam, S.S.; McCutcheon, J.R. Increasing strength of electrospun nanofiber membranes for water filtration using solvent vapor. *J. Membr. Sci.* **2013**, *436*, 213–220. [CrossRef]
55. Chen, X.; Cao, Q.; Chen, T.; Wang, D.; Fan, Y.; Xing, W. 3D printing for precision construction of ceramic membranes: Current status, challenges, and prospects. *Adv. Membr.* **2023**, *3*, 100068. [CrossRef]
56. Zakeri, S.; Vippola, M.; Levänen, E. A comprehensive review of the photopolymerization of ceramic resins used in stereolithography. *Addit. Manuf.* **2020**, *35*, 101177. [CrossRef]
57. Li, J.; Boyer, C.; Zhang, X. 3D printing based on photopolymerization and photocatalysts: Review and prospect. *Macromol. Mater. Eng.* **2022**, *307*, 2200010. [CrossRef]
58. Masciandaro, S.; Torrell, M.; Leone, P.; Tarancón, A. Three-dimensional printed yttria-stabilized zirconia self-supported electrolytes for solid oxide fuel cell applications. *J. Eur. Ceram. Soc.* **2019**, *39*, 9–16. [CrossRef]
59. Pesce, A.; Hornés, A.; Núñez, M.; Morata, A.; Torrell, M.; Tarancón, A. 3D printing the next generation of enhanced solid oxide fuel and electrolysis cells. *J. Mater. Chem. A* **2020**, *8*, 16926–16932. [CrossRef]
60. Qin, H.; Guo, W.; Huang, X.; Gao, P.; Xiao, H. Preparation of yttria-stabilized ZrO_2 nanofiltration membrane by reverse micelles-mediated sol-gel process and its application in pesticide wastewater treatment. *J. Eur. Ceram. Soc.* **2020**, *40*, 145–154. [CrossRef]
61. Coppola, B.; Lacondemine, T.; Tardivat, C.; Montanaro, L.; Palmero, P. Designing alumina-zirconia composites by DLP-based stereolithography: Microstructural tailoring and mechanical performances. *Ceram. Int.* **2021**, *47*, 13457–13468. [CrossRef]
62. Chen, F.; Zhu, H.; Wu, J.-M.; Chen, S.; Cheng, L.-J.; Shi, Y.-S.; Mo, Y.-C.; Li, C.-H.; Xiao, J. Preparation and biological evaluation of ZrO2 all-ceramic teeth by DLP technology. *Ceram. Int.* **2020**, *46*, 11268–11274. [CrossRef]
63. Zhou, M.; Liu, W.; Wu, H.; Song, X.; Chen, Y.; Cheng, L.; He, F.; Chen, S.; Wu, S. Preparation of a defect-free alumina cutting tool via additive manufacturing based on stereolithography–Optimization of the drying and debinding processes. *Ceram. Int.* **2016**, *42*, 11598–11602. [CrossRef]
64. Goswami, A.; Ankit, K.; Balashanmugam, N.; Umarji, A.M.; Madras, G. Optimization of rheological properties of photopolymerizable alumina suspensions for ceramic microstereolithography. *Ceram. Int.* **2014**, *40*, 3655–3665. [CrossRef]
65. Gentry, S.P.; Halloran, J.W. Depth and width of cured lines in photopolymerizable ceramic suspensions. *J. Eur. Ceram. Soc.* **2013**, *33*, 1981–1988. [CrossRef]
66. Chartier, T.; Badev, A.; Abouliatim, Y.; Lebaudy, P.; Lecamp, L. Stereolithography process: Influence of the rheology of silica suspensions and of the medium on polymerization kinetics–cured depth and width. *J. Eur. Ceram. Soc.* **2012**, *32*, 1625–1634. [CrossRef]
67. Tomeckova, V.; Halloran, J.W. Critical energy for photopolymerization of ceramic suspensions in acrylate monomers. *J. Eur. Ceram. Soc.* **2010**, *30*, 3273–3282. [CrossRef]
68. Wozniak, M.; de Hazan, Y.; Graule, T.; Kata, D. Rheology of UV curable colloidal silica dispersions for rapid prototyping applications. *J. Eur. Ceram. Soc.* **2011**, *31*, 2221–2229. [CrossRef]
69. Yu, M.; Feng, Q.; Liu, Z.; Zhang, P.; Zhu, X.; Mu, S. Recent Novel Fabrication Techniques for Proton-Conducting Solid Oxide Fuel Cells. *Crystals* **2024**, *14*, 225. [CrossRef]
70. Xing, B.; Cao, C.; Zhao, W.; Shen, M.; Wang, C.; Zhao, Z. Dense 8 mol% yttria-stabilized zirconia electrolyte by DLP stereolithography. *J. Eur. Ceram. Soc.* **2020**, *40*, 1418–1423. [CrossRef]
71. Xing, B.; Yao, Y.; Meng, X.; Zhao, W.; Shen, M.; Gao, S.; Zhao, Z. Self-supported yttria-stabilized zirconia ripple-shaped electrolyte for solid oxide fuel cells application by digital light processing three-dimension printing. *Scr. Mater.* **2020**, *181*, 62–65. [CrossRef]
72. Svetlizky, D.; Das, M.; Zheng, B.; Vyatskikh, A.L.; Bose, S.; Bandyopadhyay, A.; Schoenung, J.M.; Lavernia, E.J.; Eliaz, N. Directed energy deposition (DED) additive manufacturing: Physical characteristics, defects, challenges and applications. *Mater. Today* **2021**, *49*, 271–295. [CrossRef]
73. Dezaki, M.L.; Serjouei, A.; Zolfagharian, A.; Fotouhi, M.; Moradi, M.; Ariffin, M.; Bodaghi, M. A review on additive/subtractive hybrid manufacturing of directed energy deposition (DED) process. *Adv. Powder Mater.* **2022**, *1*, 100054. [CrossRef]
74. Jinoop, A.; Paul, C.; Mishra, S.; Bindra, K. Laser Additive Manufacturing using directed energy deposition of Inconel-718 wall structures with tailored characteristics. *Vacuum* **2019**, *166*, 270–278. [CrossRef]
75. Mu, S.; Hong, Y.; Huang, H.; Ishii, A.; Lei, J.; Song, Y.; Li, Y.; Brinkman, K.S.; Peng, F.; Xiao, H. A novel laser 3D printing method for the advanced manufacturing of protonic ceramics. *Membranes* **2020**, *10*, 98. [CrossRef] [PubMed]
76. Hong, Y.; Lei, J.; Heim, M.; Song, Y.; Yuan, L.; Mu, S.; Bordia, R.K.; Xiao, H.; Tong, J.; Peng, F. Fabricating ceramics with embedded microchannels using an integrated additive manufacturing and laser machining method. *J. Am. Ceram. Soc.* **2019**, *102*, 1071–1082. [CrossRef]

77. Ishii, A.; Mu, S.; Meng, Y.; Huang, H.; Lei, J.; Li, Y.; Peng, F.; Xiao, H.; Tong, J.; Brinkman, K.S. Rapid Laser Processing of Thin Sr-Doped LaCrO3–δ Interconnects for Solid Oxide Fuel Cells. *Energy Technol.* **2020**, *8*, 2000364. [CrossRef]
78. Mu, S.; Huang, H.; Ishii, A.; Zhao, Z.; Zou, M.; Kuzbary, P.; Peng, F.; Brinkman, K.S.; Xiao, H.; Tong, J. Rapid laser reactive sintering of BaCe0. 7Zr0. 1Y0. 1Yb0. 1O3-δ electrolyte for protonic ceramic fuel cells. *J. Power Sources Adv.* **2020**, *4*, 100017. [CrossRef]
79. Mu, S.; Zhao, Z.; Huang, H.; Lei, J.; Peng, F.; Xiao, H.; Brinkman, K.S.; Tong, J.J. Advanced Manufacturing of Intermediate-Temperature Protonic Ceramic Electrochemical Cells. *Electrochem. Soc. Interface* **2020**, *29*, 67. [CrossRef]
80. Shahzad, A.; Lazoglu, I. Direct ink writing (DIW) of structural and functional ceramics: Recent achievements and future challenges. *Compos. Part B Eng.* **2021**, *225*, 109249. [CrossRef]
81. Yang, J.; Xiao, Z.; Chen, J.; Zhang, S. Study on process parameters and structural angles of printed part of slurry extrusion ceramic 3D printing. *Manuf. Technol. Mach. Tool* **2023**, *6*, 11–15.
82. Wang, H.; Wang, X.; Meng, B.; Tan, X.; Loh, K.S.; Sunarso, J.; Liu, S. Perovskite-based mixed protonic–electronic conducting membranes for hydrogen separation: Recent status and advances. *J. Ind. Eng. Chem.* **2018**, *60*, 297–306. [CrossRef]
83. Abdeljawad, F.; Bolintineanu, D.S.; Cook, A.; Brown-Shaklee, H.; DiAntonio, C.; Kammler, D.; Roach, A. Sintering processes in direct ink write additive manufacturing: A mesoscopic modeling approach. *Acta Mater.* **2019**, *169*, 60–75. [CrossRef]
84. Sun, D.; Lu, Y.; Karaki, T. Review of the applications of 3D printing technology in the field of piezoelectric ceramics. *Resour. Chem. Mater.* **2023**, *2*, 128–142. [CrossRef]
85. Derby, B. Additive manufacture of ceramics components by inkjet printing. *Engineering* **2015**, *1*, 113–123. [CrossRef]
86. Hoth, C.N.; Schilinsky, P.; Choulis, S.A.; Brabec, C.J. Printing highly efficient organic solar cells. *Nano Lett.* **2008**, *8*, 2806–2813. [CrossRef] [PubMed]
87. Choulis, S.A.; Hoth, C.N.; Schilinsky, P. High photovoltaic performance of inkjet printed polymer: Fullerene blends. *Adv. Mater.* **2007**, *19*, 3973–3978.
88. Lavery, L.L.; Whiting, G.L.; Arias, A.C. All ink-jet printed polyfluorene photosensor for high illuminance detection. *Org. Electron.* **2011**, *12*, 682–685. [CrossRef]
89. Dua, V.; Surwade, S.P.; Ammu, S.; Agnihotra, S.R.; Jain, S.; Roberts, K.E.; Park, S.; Ruoff, R.S.; Manohar, S.K. All-organic vapor sensor using inkjet-printed reduced graphene oxide. *Angew. Chem.* **2010**, *122*, 2200–2203. [CrossRef]
90. Correia, V.; Mitra, K.; Castro, H.; Rocha, J.; Sowade, E.; Baumann, R.; Lanceros-Méndez, S. Design and fabrication of multilayer inkjet-printed passive components for printed electronics circuit development. *J. Manuf. Process.* **2018**, *31*, 364–371. [CrossRef]
91. Kang, B.J.; Lee, C.K.; Oh, J.H. All-inkjet-printed electrical components and circuit fabrication on a plastic substrate. *Microelectron. Eng.* **2012**, *97*, 251–254. [CrossRef]
92. He, Z.; Shanmugasundaram, T.; Singh, G. Inkjet 3D printing of clay ceramics for water treatment. *Prog. Addit. Manuf.* **2018**, *3*, 215–219. [CrossRef]
93. Karunakaran, S.K.; Arumugam, G.M.; Yang, W.; Ge, S.; Khan, S.N.; Lin, X.; Yang, G. Recent progress in inkjet-printed solar cells. *J. Mater. Chem. A* **2019**, *7*, 13873–13902. [CrossRef]
94. Wang, C.; Park, M.J.; Choo, Y.W.; Huang, Y.; Phuntsho, S.; Shon, H.K. Inkjet printing technique for membrane fabrication and modification: A review. *Desalination* **2023**, *565*, 116841. [CrossRef]
95. Cano-Vicent, A.; Tambuwala, M.M.; Hassan, S.S.; Barh, D.; Aljabali, A.A.; Birkett, M.; Arjunan, A.; Serrano-Aroca, Á. Fused deposition modelling: Current status, methodology, applications and future prospects. *Addit. Manuf.* **2021**, *47*, 102378. [CrossRef]
96. Dev, S.; Srivastava, R. Optimization of fused deposition modeling (FDM) process parameters for flexural strength. *Mater. Today Proc.* **2021**, *44*, 3012–3016. [CrossRef]
97. Dermeik, B.; Travitzky, N. Laminated object manufacturing of ceramic-based materials. *Adv. Eng. Mater.* **2020**, *22*, 2000256. [CrossRef]
98. Gupta, R.; Dalakoti, M.; Narasimhulu, A. A critical review of process parameters in laminated object manufacturing process. In *Advances in Materials Engineering and Manufacturing Processes: Select Proceedings of ICFTMM*; Springer: Singapore, 2020; pp. 31–39.
99. Weisensel, L.; Travitzky, N.; Sieber, H.; Greil, P. Laminated object manufacturing (LOM) of SiSiC composites. *Adv. Eng. Mater.* **2004**, *6*, 899–903. [CrossRef]
100. Rossnagel, S. Thin film deposition with physical vapor deposition and related technologies. *J. Vac. Sci. Technol. A Vac. Surf. Film.* **2003**, *21*, S74–S87. [CrossRef]
101. Mahan, J.E. *Physical Vapor Deposition of Thin Films*; Wiley-VCH: Weinheim, Germany, 2000.
102. Wang, X.; Jiang, M.; Zhou, Z.; Gou, J.; Hui, D. 3D printing of polymer matrix composites: A review and prospective. *Compos. Part B Eng.* **2017**, *110*, 442–458. [CrossRef]
103. Wohlers, T. *3D Printing and Additive Manufacturing State of the Industry: Annual Worldwide Progress Report Wohlers Report*; The Middle East, and Other Countries, Wohlers Associates: Fort Collins, CO, USA, 2017; p. 344.
104. Mu, S.; Huang, H.; Ishii, A.; Hong, Y.; Santomauro, A.; Zhao, Z.; Zou, M.; Peng, F.; Brinkman, K.S.; Xiao, H. Rapid laser reactive sintering for sustainable and clean preparation of protonic ceramics. *ACS Omega* **2020**, *5*, 11637–11642. [CrossRef]
105. Rasaki, S.; Liu, C.; Lao, C.; Zhang, H.; Chen, Z. The innovative contribution of additive manufacturing towards revolutionizing fuel cell fabrication for clean energy generation: A comprehensive review. *Renew. Sustain. Energy Rev.* **2021**, *148*, 111369. [CrossRef]

106. Feng, Z.; Liu, L.; Li, L.; Chen, J.; Liu, Y.; Li, Y.; Hao, L.; Wu, Y. 3D printed Sm-doped ceria composite electrolyte membrane for low temperature solid oxide fuel cells. *Int. J. Hydrogen Energy* **2019**, *44*, 13843–13851. [CrossRef]
107. Wei, L.; Zhang, J.; Yu, F.; Zhang, W.; Meng, X.; Yang, N.; Liu, S. A novel fabrication of yttria-stabilized-zirconia dense electrolyte for solid oxide fuel cells by 3D printing technique. *Int. J. Hydrogen Energy* **2019**, *44*, 6182–6191. [CrossRef]
108. Qi, K.; Chen, M.; Dai, R.; Li, Q.; Lai, M.; Wang, Z. Development of an electrochemical ceramic membrane bioreactor for the removal of PPCPs from wastewater. *Water* **2020**, *12*, 1838. [CrossRef]
109. Zheng, J.; Xu, S.; Wu, Z.; Wang, Z. Removal of p-chloroaniline from polluted waters using a cathodic electrochemical ceramic membrane reactor. *Sep. Purif. Technol.* **2019**, *211*, 753–763. [CrossRef]
110. Huang, W.; Finnerty, C.; Sharp, R.; Wang, K.; Balili, B. High-performance 3D printed microtubular solid oxide fuel cells. *Adv. Mater. Technol.* **2017**, *2*, 1600258. [CrossRef]
111. Bae, K.; Noh, H.-S.; Jang, D.Y.; Hong, J.; Kim, H.; Yoon, K.J.; Lee, J.-H.; Kim, B.-K.; Shim, J.H.; Son, J.-W. High-performance thin-film protonic ceramic fuel cells fabricated on anode supports with a non-proton-conducting ceramic matrix. *J. Mater. Chem. A* **2016**, *4*, 6395–6403. [CrossRef]
112. Fan, Z.; Li, L.; Mei, X.; Zhao, F.; Li, H.; Zhuo, X.; Zhang, X.; Lu, Y.; Zhang, L.; Liu, M. Multilayer ceramic film capacitors for high-performance energy storage: Progress and outlook. *J. Mater. Chem. A* **2021**, *9*, 9462–9480. [CrossRef]
113. Pan, M.-J.; Randall, C.A. A brief introduction to ceramic capacitors. *IEEE Electr. Insul. Mag.* **2010**, *26*, 44–50. [CrossRef]
114. Niedrach, L.W. A New Membrane-Type pH Sensor for Use in High Temperature-High Pressure Water. *J. Electrochem. Soc.* **1980**, *127*, 2122. [CrossRef]
115. Jurków, D.; Maeder, T.; Dąbrowski, A.; Santo Zarnik, M.; Belavič, D.; Bartsch, H.; Müller, J. Overview on low temperature co-fired ceramic sensors. *Sens. Actuators A Phys.* **2015**, *233*, 125–146. [CrossRef]